Spring 5-31-2005

Electromagnetic and acoustic propagation in strip lines and porous media

Lin Zhou
New Jersey Institute of Technology

ABSTRACT

ELECTROMAGNETIC AND ACOUSTIC PROPAGATION IN STRIP LINES AND POROUS MEDIA

by
Lin Zhou

Wave propagation in two physical structures is described and analyzed in this dissertation. In the first problem, the propagation of a normally incident plane acoustic wave through a three dimensional rigid slab with periodically placed holes is modeled and analyzed. The spacing of the holes A and B, the wavelength λ and the thickness of the slab L are order one parameters compared to the characteristic size D of the holes, which is a small quantity. Scattering matrix techniques are used to derive expressions for the transmission and reflection coefficients of the lowest mode. These expressions depend only on the transmission coefficient, τ_0, of an infinitely long slab with the same configuration. The determination of τ_0 requires the solution of an infinite set of algebraic equations. These equations are approximately solved by exploiting the small parameter $D/\sqrt{AB}$. Remarkably, this structure is transparent at certain frequencies which could prove useful in narrow band filters and resonators.

In the second problem, a systematic mathematical approach is given to find the solutions of microstrip transmission lines. Specifically, we employ an asymptotic method to determine an approximation to the field components and propagation constant when the wavelength is much bigger than the thickness of the substrate. It is found that the transverse electrical and magnetic fields can be expressed in terms of two potential functions which are elliptic in character and are coupled through the longitudinal electrical field boundary conditions. The solvability conditions for the longitudinal magnetic field yield an approximation to the propagation constant. Transmission line equations are also obtained for coupled microstrip transmission lines and single microstrips with smoothly changing widths by using the same techniques.

ELECTROMAGNETIC AND ACOUSTIC PROPAGATION IN STRIP LINES AND POROUS MEDIA

by
Lin Zhou

A Dissertation
Submitted to the Faculty of
New Jersey Institute of Technology and
Rutgers, The State University of New Jersey – Newark
in Partial Fulfillment of the Requirements for the Degree of
Doctor of Philosophy in Mathematical Sciences

Department of Mathematical Sciences
Department of Mathematics and Computer Science, Rutgers-Newark

May 2005

APPROVAL PAGE

ELECTROMAGNETIC AND ACOUSTIC PROPAGATION IN STRIP LINES AND POROUS MEDIA

Lin Zhou

Gregory A. Kriegsmann, Ph.D, Dissertation Advisor — Date
Distinguished Professor, Department of Mathematical Sciences, NJIT

Peter G. Petropoulos, Ph.D, Dissertation Co-Advisor — Date
Associate Professor, Department of Mathematical Sciences, NJIT

Demetrius T. Papageorgiou, Ph.D, Committee Member — Date
Professor, Department of Mathematical Sciences, NJIT

Jonathan H. C. Luke, Ph.D, Committee Member — Date
Professor, Department of Mathematical Sciences, NJIT

Gerald Whitman, Ph.D, Committee Member — Date
Professor, Department of Electrical and Computer Engineering, NJIT

BIOGRAPHICAL SKETCH

Author: Lin Zhou

Degree: Doctor of Philosophy

Date: May 2005

Undergraduate and Graduate Education:

- Doctor of Philosophy in Mathematical Sciences,
  New Jersey Institute of Technology, Newark, NJ, 2005
- Master of Science in Applied Mathematics,
  New Jersey Institute of Technology, Newark, NJ, 2004
- Master of Science in Noise Control Engineering,
  Beijing Municipal Institute of Labor Protection, Beijing, China, Jun 1999
- Bachelor of Science in Electrical Sciences and Engineering,
  Nanjing University, Nanjing, China, July 1996

Major: Applied Mathematics

To my husband, Xu Wugang and my mother, Jin Zhiwen

ACKNOWLEDGMENT

I give my special thanks to my advisor Dr. Gregory Kriegsmann for his valuable ideas and his untiring guidance. I greatly appreciate his generosity with time, his inspiring suggestions and encouragement.

I am grateful to Dr. Peter Petropoulos for agreeing to be my co-advisor, for his help specially in the computational aspects of my dissertation and for his advice.

I am very thankful to Dr. Demetrius Papageorgiou, Dr. Gerald Whitman and Dr. Jonathan Luke for agreeing to be on my committee and for their support during my research at NJIT.

Sincere thanks to Dr. Daljit Ahluwalia for his support and his advice throughout my stay at NJIT. Thanks to him and the department for their generous financial support. I thank all the faculty in the Department of Mathematical Sciences at NJIT for imparting their knowledge and for the many mathematical discussions with them.

I would also like to thank Ms. Roseanne Rowan for her cooperation and help with administrative complexities.

Thanks to my best friend Dr. Jyoti Champanerkar, who accompanied me throughout my graduate school and helped me with my English. I also thank my friend, Muhammad Hameed, for his support and for sharing his knowledge.

Finally, I take this opportunity to express my deep gratitude to my beloved husband, Xu Wugang and my mom, Jin Zhiwen for their love and for their faith in me. Without them I would not have been able to accomplish this.

TABLE OF CONTENTS

TABLE OF CONTENTS
(Continued)

Chapter **Page**

LIST OF FIGURES

LIST OF FIGURES
(Continued)

Figure **Page**

CHAPTER 1

INTRODUCTION

1.1 Problem Statement

Wave propagation through complex structures is an important topic in many scientific and technological fields. In most cases, analytic solutions are not available. The corresponding mathematical problems have to be solved approximately to understand the propagation phenomena.

In this dissertation, wave propagation in two physical structures is described and analyzed. The first problem is concerned with a normally incident acoustic wave propagation through a periodically perforated rigid slab. This problem is a model of wave propagation through porous media. The second problem is concerned with an electromagnetic wave propagation in microstrip transmission lines, which arises from microwave integrated circuits. Both of the geometries are complicated so that exact solutions are not available. Therefore, we have developed new approaches to solve these two problems approximately.

Specifically, for the first problem, scattering matrix theory is applied to find the transmitted and the reflected acoustic waves of the slab structure. Two auxiliary problems are analyzed to obtain the entries of the scattering matrix. By using the unitary character of the scattering matrix of the first auxiliary problem, the problem of the slab is greatly simplified. Numerical solutions are obtained for small holes. Some interesting phenomena of complete transmission are found independent of the shape of the holes, which make the structure useful in constructing narrow band filters and resonators.

For the second problem, a perturbation analysis is directly applied to Maxwell equations for microstrip transmission lines in the case when the wavelength is much

bigger than the size of the strip. By solving each order of the fields' equations, transmission line equations are derived and each term in the equation is interpreted mathematically. The method can be generalized to the microstrip transmission lines with different configurations. This systematic mathematical derivation also gives an approximation to the propagation constant of the microstrip transmission lines.

1.2 Dissertation Overview

This dissertation is organized in the following way. Chapters 2 and 3 include the first problem. In Chapter 2, a mathematical formulation of the first problem is presented under certain assumptions. Two auxiliary problems are analyzed and are used to find the scattering matrix S of the slab structure. By using this matrix S we are able to describe the properties of the transmitted waves and the reflected waves of the slab. It turns out that the transmission coefficient of the lowest mode of the slab structure depends on only one parameter τ_0, which is the transmission coefficient of the first auxiliary problem. All the results in this chapter are for holes of arbitrary shapes.

In Chapter 3, the transmission properties of the slab structure are discussed by finding τ_0. The determination of τ_0 requires the solution of an infinite set of algebraic equations. Under the assumption that the size of the holes is much smaller than the spacing of the holes, these equations are approximately solved by exploiting the small parameter $D/\sqrt{AB}$ for circular and rectangular holes, respectively. The transmission coefficients and the reflection coefficients are plotted as functions of frequency to show the frequency selecting properties of the structure. This chapter ends with the conclusion of the first problem.

Chapters 4, 5 and 6 contain the second problem of microstrip transmission lines. In Chapter 4, the dispersive properties of a single microstrip transmission line are analyzed by a perturbation method. Specifically, we find the asymptotic expansions of the electromagnetic fields and the propagation constant for the case

when the wavelength is much larger than the height of the substrate (low frequency approximation). The first several terms of the electrical and magnetic fields and the propagation constant are found in terms of potential functions. Some important results are obtained through this systematic derivations. The Padé approximation is used to derive the propagation constant as a function of frequencies.

In Chapter 5, the derived potential problems are solved numerically and the propagation constant is found. Specifically, these potential problems are converted into integral equations by applying the corresponding Green's functions, and these integral equations are solved by Garlerkin's method. The results are compared with those obtained by other authors.

In Chapter 6, we generalize our approach to analyze the case when the strip width smoothly changes in the direction of propagation and the case of coupled uniform microstrip transmission lines. For the variable width strip line, we obtain a transmission line equation for the potential along the strip. For the coupled microstrip transmission lines, coupled transmission line equations are derived for potentials and currents along the two strips with each coefficient being properly defined through the known potential functions. The chapter ends with the conclusion of the problem.

Some of the technical derivations are left out of the main chapters to preserve the flow of ideas. These details are included in the six appendices, Appendix A through Appendix F after Chapter 6, at the end of the dissertation.

CHAPTER 2

SCATTERING MATRIX METHOD

2.1 Introduction

The propagation of electromagnetic waves through metallic grating structures has been studied both experimentally [9], [14] and theoretically [4], [31], [28], [30] in recent years. Metallic grating structures have the properties of complete transmission at certain frequencies, which make these structures useful in photonic and microwave circuits. In [20], Kriegsmann addresses the problem of a TM polarized electromagnetic wave through a 2-dimensional periodic structure. Resonant properties of the structure are explained in [20] using the scattering matrix method.

The scattering matrix method is also suitable to study a similar acoustic problem. The acoustic analog of the electromagnetic problem consists of investigating the propagation of acoustic waves through porous media in which the pores are periodically distributed. In [25], Norris examines the frequency responses for an infinitely long, rigid structure perforated with circular holes. Total reflection is found at certain frequencies up to the first cut-off frequency.

In this dissertation, the acoustic transmission properties of a structure of finite length, and otherwise similar to the one examined in [25], are considered by applying the scattering matrix method. The scattering matrix of the structure, which depends on only one parameter, is derived for arbitrarily shaped holes. Under the assumption that the incident wavelength is of the same order as the spacing of the holes and is much bigger than the hole size, the total transmission and total reflection properties of the structure at certain frequencies are obtained for both circular and rectangular holes. Some of the results obtained here are also found in [25]. However, the derivations in this dissertation are more straight forward and the results are obtained

for general hole shapes. The frequency selection property of the structure makes itself useful in constructing narrow band filters and resonators.

The problem is illustrated in Figure 2.1 and discussed in Chapters 2 and 3. In Section 2.2, the mathematical formulation of the problem is presented and the assumptions made are stated. This is followed by modal solutions to each part of the structure. The solution outside the holes is explicit. The solution inside the holes depends on the shape of the holes. However, the lowest eigenvalue and the eigenfunction for different shapes are found to be the same. In Section 2.3, we describe the scattering matrix method and deduce a scattering matrix S for the structure. This allows both the transmission and the reflection coefficients to be obtained using S. In deriving S, two auxiliary problems are introduced and discussed. It turns out that the scattering matrix S depends on only one complex coefficient τ_0, which is the transmission coefficient for the first auxiliary problem. The unitary character of S forces τ_0 to lie on a circle in the complex plane.

2.2 Mathematical Formulation

A schematic diagram of the structure is shown in Figure 2.1. It is a rigid slab, infinitely long in both X and Y directions. In the Z direction the thickness of the slab is L. Holes are arranged periodically in the XY plane, and the cross section of the hole is uniform along the Z direction. All the holes are of the same shape. Since the structure is periodic, we consider a fundamental cell which is also shown in Figure 2.1. The length and the width of the fundamental cell are A and B, respectively. For an arbitrarily shaped hole, we define D, the square root of the hole's area, as the characteristic size of the hole.

A plane acoustic wave with frequency ω is normally incident on the rigid material (in this problem, the wave is assumed to be of the form $e^{-i\omega t}$). The incident wavelengh λ is of the same order as A and B. We assume that the viscosity of

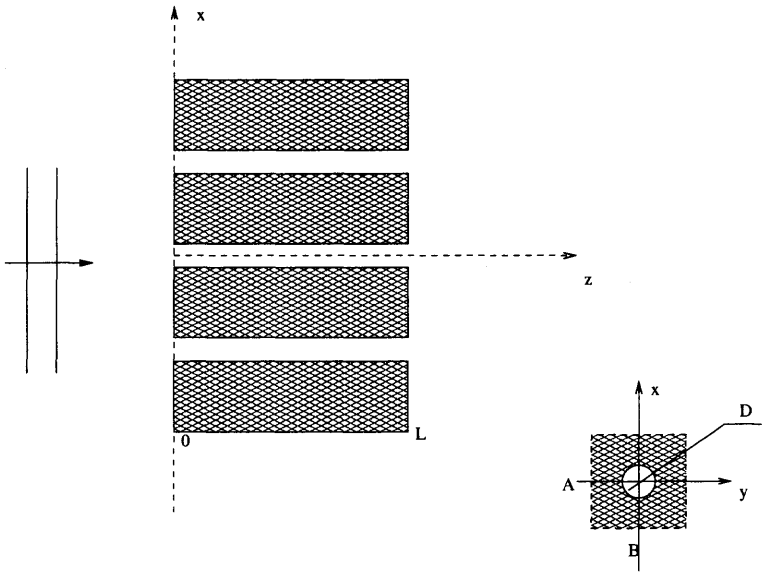

Figure 2.1 Schematic diagram of the periodic structure considered in problem 1.

air is small enough so that the boundary layer on the surface of the hole channel can be neglected. Therefore, the acoustic pressure U satisfies Helmholtz equation, $\nabla^2 U + K^2 U = 0$ both inside the hole and outside the slab. The constant K in the Helmholtz equation is the wavenumber defined as $K = 2\pi/\lambda$. The boundary condition is $\partial U/\partial n = 0$ on the rigid material, where n denotes the normal direction to the rigid surfaces.

We assume that the hole is small compared to the size of the fundamental cell. That is, $D << \sqrt{AB}$. Under this assumption, it is intuitive that most of the incident wave will be reflected from the slab and only a small remnant of the wave will be able to reach the region $Z > L$.

All upper case letters used so far are dimensional parameters and variables. We will use lower case letters to denote the corresponding dimensionless quantities. We scale all lengths by $\sqrt{AB}$. Therefore, the fundamental cell has length a and width b, and $ab = 1$. The slab thickness $l = L/\sqrt{AB}$, which is an order one parameter in our problem. The wavenumber $k = K\sqrt{AB}$ and the characteristic size of the hole is $d = D/\sqrt{AB}$. The assumption $D << \sqrt{AB}$ explained above, implies that

$d << 1$. The pressure U is scaled by the amplitude of the incident wave. After nondimensionalization, the governing equation and the boundary condition become

$$\begin{aligned} \nabla^2 u + k^2 u &= 0, \\ \frac{\partial u}{\partial n} &= 0. \end{aligned} \tag{2.1}$$

Since the structure is periodic, with a normally incident wave, it is expected that in regions $z < 0$ and $z > l$, both u and its normal derivative are periodic functions of x and y with period a and b, respectively. By applying the boundary conditions, the solutions in regions $z < 0$ and $z > l$ can be written as eigenfunction expansions,

$$u(x,y,z) = e^{ikz}\psi_{00} + \sum_{m=0}^{\infty}\sum_{n=0}^{\infty} R_{mn}\psi_{mn}(x,y)e^{-i\beta_{mn}z} \qquad z < 0, \tag{2.2a}$$

$$u(x,y,z) = \sum_{m=0}^{\infty}\sum_{n=0}^{\infty} T_{mn}\psi_{mn}(x,y)e^{i\beta_{mn}z} \qquad z > l. \tag{2.2b}$$

In the region $z < 0$, the solution consists of the incident wave $u_i = e^{ikz}$ and reflected waves. The unknowns R_{mn} are the amplitudes of the mn^{th} reflected modes and β_{mn} are the corresponding propagation constants. In the region $z > l$, the mn^{th} mode of the transmitted wave has an unknown amplitude T_{mn}. In (2.2a) and (2.2b) ψ_{mn} are normalized eigenfunctions of the periodic structure. If we choose the origin of the coordinate system to be at the center of the fundamental cell, these eigenfunctions can be written explicitly as

$$\psi_{00} = 1, \tag{2.3a}$$

$$\psi_{0n} = \sqrt{2}\cos\frac{2n\pi y}{b}, \qquad \psi_{m0} = \sqrt{2}\cos\frac{2m\pi x}{a}, \tag{2.3b}$$

$$\psi_{mn} = 2\cos\frac{2m\pi x}{a}\cos\frac{2n\pi y}{b} \qquad m,n = 1,2,3\cdots, \tag{2.3c}$$

and the propagation constants are

$$\beta_{mn} = \sqrt{k^2 - \frac{4m^2\pi^2}{a^2} - \frac{4n^2\pi^2}{b^2}} \qquad m,n = 0,1,2\cdots. \tag{2.4}$$

In the channel where $0 < z < l$, there are waves in both z and $-z$ directions. If we can find the eigenvalues and eigenfunctions corresponding to a particular shape, we can write down the solution of the Helmholtz equation in terms of the eigenvalues and eigenfunctions in this region, just as we did for the regions outside the slab. We know that for the Laplace operator with a Neumann boundary condition, all eigenvalues are real and positive, therefore the eigenvalues can be ordered. Let λ_p denote the eigenvalues and φ_p denote the corresponding eigenfunctions, where $p = 0, 1, 2, \cdots$, then the solution in the channel can be expressed as

$$u(x, y, z) = \sum_{p=0}^{\infty} (A_p e^{-ik_p z} + B_p e^{ik_p z}) \varphi_p(x, y) \qquad 0 < z < l. \tag{2.5}$$

In equation (2.5) the propagation constants k_p are defined as $k_p = \sqrt{k^2 - \lambda_p^2}$, and the amplitudes A_p and B_p of each mode are unknown. Although the eigenvalues and eigenfunctions depend on the shape of the hole, the smallest eigenvalue and its corresponding normalized eigenfunction are the same for all shapes. The smallest eigenvalue is $\lambda_0 = 0$ and its corresponding eigenfunction is $\varphi_0 = 1/d$. Therefore, we have

$$k_0 = k, \tag{2.6a}$$

$$\varphi_0 = \frac{1}{d}. \tag{2.6b}$$

All the eigenvalues λ_p for $p \geq 1$ are greater than 0 and of order $1/d$. (The proof of the preceeding statement is detailed in Appendix A). If we choose k such that only the lowest mode can propagate in the channel, then $k_p = i\sqrt{\lambda_p^2 - k^2}$ for $p \geq 1$. Since $d << 1$, these eigenvalues λ_p are much greater than k. Therefore, the propagation constants k_p can be approximated by

$$k_p \approx i\tilde{\lambda}_p/d, \qquad p = 1, 2 \cdots \tag{2.7}$$

with $\tilde{\lambda}_p$ being order one quantities. This means that all the higher modes in the hole channel are highly damped.

2.3 The Method

2.3.1 Scattering Matrix Method

In Section 2.2, we derived solutions of the slab problem in terms of eigenfunction expansions. By finding the unknown coefficients of each mode, the problem will be solved completely. One way to find the unknown coefficients is by using the boundary conditions that connect the three regions, $z < 0$, $0 < z < l$ and $z > l$. This can be attained by using Green's function arguments to derive two integral equations, one at $z = 0$ and the other at $z = l$, and substituting these modal solutions in the integral equations. Then, by exploiting the orthonormal properties of eigenfunctions, two coupled infinite systems of algebraic equations can be derived and solved numerically to obtain the transmission coefficients T_{mn} and the reflection coefficients R_{mn}.

The other approach to solve the problem, as is illustrated in this dissertation, is by the application of the scattering matrix method. In microwave circuit analysis and design, the scattering matrix is widely used to characterize a component , such as, an amplifier or a magic-T, in a circuit [12]. As shown in Figure 2.2, a two-port component in a circuit has two inputs and two outputs with amplitudes a_0, b_0, c_0 and d_0. The outputs of this component are connected to the inputs through a matrix

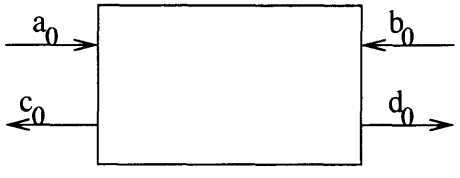

Figure 2.2 A typical component of microwave circuits.

S, which is often obtained experimentally. That is, the inputs and the outputs are

related by the following equation,

$$\begin{bmatrix} c_0 \\ d_0 \end{bmatrix} = \begin{bmatrix} S_{11} & S_{12} \\ S_{21} & S_{22} \end{bmatrix} \begin{bmatrix} a_0 \\ b_0 \end{bmatrix} = S \begin{bmatrix} a_0 \\ b_0 \end{bmatrix}. \tag{2.8}$$

Once the scattering matrix S of the device is known, and any two amplitudes, such as a_0 and b_0 are known, the remaining two amplitudes c_0 and d_0 can be found using equation (2.8).

Therefore, we are going to construct a scattering matrix to the slab problem, which connects the lowest mode of transmitted and reflected waves to the incident waves. In order to do so, we will divide the slab into two parts at $z = l/2$. A scattering matrix for each part will be constructed individually. Then, by combining these two matrices, the scattering matrix for the slab structure will be obtained.

We assume that $k < 2\pi/a$ if $a > b$, otherwise $k < 2\pi/b$, then all k_p for $p \geq 1$ are imaginary according to equation (2.7). The modes with imaginary propagation constants damp exponentially. Thus, only one mode propagates in the channel. If we assume that the channel is long enough so that at $z = l/2$, all damping modes are exponentially small and negligible, then at $z = l/2$, the acoustic field can be written as follows,

$$u = (A_0 e^{-ikz} + B_0 e^{ikz})\varphi_0. \tag{2.9}$$

For this value of k, there is only one reflected mode in the region $z < 0$ which can propagate. Hence, at a distance several wavelengths to the left of the aperture $z = 0$, the field is

$$u = (e^{ikz} + R_{00} e^{-ikz})\psi_{00}. \tag{2.10}$$

Similarly, in the region $z > l$, only one mode is transmitted. The modal solution of the transmitted wave can be simplified as

$$u = T_{00} e^{ikz} \psi_{00}. \tag{2.11}$$

As we shall soon demonstrate, there exists a scattering matrix S_1 which connects the amplitudes of the outgoing waves R_{00} and B_0 with the amplitudes of the incident waves 1 and A_0. The scattering matrix S_1 can be considered to characterize the first half of the structure $(-\infty < z < l/2)$.

Also, we shall show that, there exists another scattering matrix S_2 which characterizes the second half of the structure $(l/2 < z < \infty)$ and connects A_0, B_0 and T_{00}. A combination of the two scattering matrices S_1 and S_2 yields the scattering matrix S of the slab.

2.3.2 Two Auxiliary Problems

In order to determine matrices S_1 and S_2, we consider two auxiliary problems. The structure of these two auxiliary problems is the same as that of the fundamental cell, except that the channel is infinitely long $(l = \infty)$.

In the first auxiliary problem, the wave is incident upon the periodic structure and is transmitted to the channel, as shown in Figure 2.3. As before, we can write a

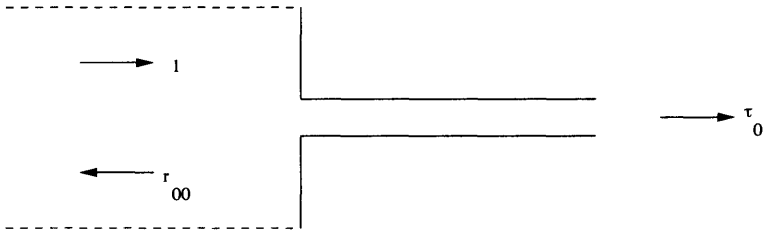

Figure 2.3 Schematic diagram illustrating the structure and the incident, reflected and transmitted waves considered in the first auxiliary problem.

modal solution of the problem as follows,

$$u_1(x,y,z) = e^{ikz}\psi_{00} + \sum_{m=0}^{\infty}\sum_{n=0}^{\infty} r_{mn}\psi_{mn}(x,y)e^{-i\beta_{mn}z} \qquad z < 0, \tag{2.12a}$$

$$u_1(x,y,z) = \sum_{p=0}^{\infty} \tau_p \varphi_p(x,y) e^{ik_p z} \qquad z > 0, \tag{2.12b}$$

in which u_1 denotes the acoustic pressure in the first auxiliary problem. In the solution given in equations (2.12), the first transmission coefficient τ_0 and the first reflection coefficient r_{00} are related by a simple equation (2.13), given below.

$$1 - r_{00} = d\tau_0 \tag{2.13}$$

Equation (2.13) is derived in the following way. To the left of $z = 0$ (at $z = -\delta$), we differentiate u_1 with respect to z, then multiply $\partial u_1/\partial z$ by ψ_{00}. After integrating it over the area of the fundamental cell and using the orthonormality of the eigenfunctions, we obtain

$$\int_{-a/2}^{a/2}\int_{-b/2}^{b/2}\left(\frac{\partial u_1}{\partial z}|_{z=-\delta}\right)\psi_{00}dxdy = ike^{-ik\delta} - ikr_{00}e^{ik\delta}. \tag{2.14}$$

Similarly, to the right of $z = 0$ (at $z = \delta$) we have

$$\iint_H \left(\frac{\partial u_1}{\partial z}|_{z=\delta}\right)\varphi_0 ds = ik\tau_0 e^{ik\delta}, \tag{2.15}$$

in which the double integral $\iint_H$ is over the area of the hole. Since at $z = 0$, function $\partial u_1/\partial z$ is zero outside the hole and is continuous across the hole, and due to the fact that $\varphi_0 d = \psi_{00}$, it follows that the left hand side of equation (2.14) is d times the left hand side of equation (2.15). Therefore, the right hand side of equation (2.14) is also d times the right hand side of equation (2.15). Taking the limit as δ approaches 0 gives equation (2.13).

The second auxiliary problem has the same structure as the first one. However, the wave is incident from the channel and is transmitted to the air region, as shown in Figure 2.4. Therefore, the modal solution to this problem is

$$u_2(x,y,z) = \sum_{m=0}^{\infty}\sum_{n=0}^{\infty}\gamma_{mn}\psi_{mn}(x,y)e^{-i\beta_{mn}z} \qquad z < 0, \tag{2.16a}$$

$$u_2(x,y,z) = e^{-ikz}\varphi_0 + \sum_{p=0}^{\infty}\rho_p\varphi_p(x,y)e^{ik_p z} \qquad z > 0. \tag{2.16b}$$

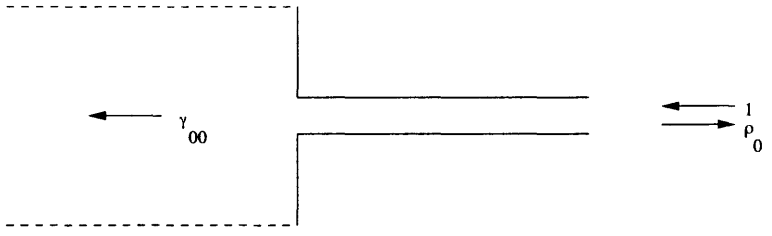

Figure 2.4 Schematic diagram illustrating the structure and the incident, reflected and transmitted waves considered in the second auxiliary problem.

Using the same argument as in the derivation of equation (2.13), it follows that the first transmission coefficient γ_{00} and the first reflection coefficient ρ_0 in the second auxiliary problem are related by

$$\gamma_{00} = d(1 - \rho_0). \tag{2.17}$$

The two auxiliary problems are not independent. Using the argument proved in Appendix B, we obtain

$$\gamma_{00} = \tau_0. \tag{2.18}$$

Equations (2.13), (2.17) and (2.18) form a system of three equations in four unknowns. Thereby, we are able to express any three parameters in terms of the fourth. Thus, if any one of the four parameters is known, the other three parameters can be easily found. Now, we let τ_0 be a known parameter and express the other three parameters, γ_{00}, r_{00} and ρ_0 in terms of τ_0.

$$r_{00} = 1 - d\tau_0 \tag{2.19a}$$

$$\rho_0 = 1 - \frac{\tau_0}{d} \tag{2.19b}$$

$$\gamma_{00} = \tau_0 \tag{2.19c}$$

The above result that any three of the four fundamental reflection and transmission coefficients can be written in terms of the fourth coefficient, is also derived in [25], in

which, a more complicated integral representation method is involved with the results holding only for circular holes.

These two auxiliary problems and their simple results enable us to find the scattering matrix of the slab which depends on only one parameter.

2.3.3 Scattering Matrix of the Slab Structure

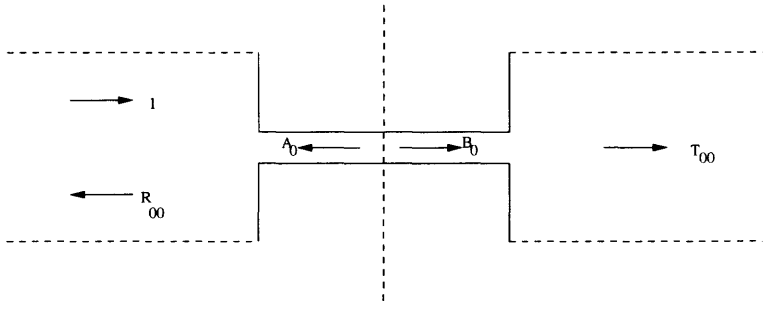

Figure 2.5 Schematic diagram illustrating the structure and the incident, reflected and transmitted waves considered in the slab structure.

Now we consider the slab problem. The scattering matrix for the first half ($-\infty < z < l/2$) is derived by linearly combining the two auxiliary problems, since both the Helmholtz equation and the boundary conditions are linear. From Figure 2.5 we observe that the first half of the structure can be viewed as having incident modes with amplitudes 1 and A_0, and reflected modes with amplitudes R_{00} and B_0. Hence, the results of the two auxiliary problems imply that

$$R_{00} = r_{00} \cdot 1 + \gamma_{00} A_0, \tag{2.20a}$$

$$B_0 = \tau_0 \cdot 1 + \rho_0 A_0. \tag{2.20b}$$

Rewriting equation (2.20) in matrix notation and using the relations given in equation (2.19) gives

$$\begin{bmatrix} R_{00} \\ B_0 \end{bmatrix} = S_1 \begin{bmatrix} 1 \\ A_0 \end{bmatrix}, \tag{2.21}$$

where the scattering matrix S_1 is

$$S_1 = \begin{bmatrix} 1 - d\tau_0 & \tau_0 \\ \tau_0 & 1 - \tau_0/d \end{bmatrix}. \tag{2.22}$$

The scattering matrix S_1 represents the first half of the slab structure. We proved in Appendix C that S_1 is a unitary matrix. Hence, τ_0 satisfies the following equation.

$$\left| \tau_0 - \frac{d}{1+d^2} \right|^2 = \left(\frac{d}{1+d^2} \right)^2 \tag{2.23}$$

The locus of equation (2.23) is a circle in the complex τ_0 plane. Using a conformal mapping, τ_0 is equivalently written as

$$\tau_0 = \frac{2d}{1 + d^2 + i\eta}, \tag{2.24}$$

where η is real and can take any value between $-\infty$ and ∞.

We now derive the scattering matrix S_2 which relates the amplitudes of incident and reflected modes at the channel opening $z = l$. We introduce a new independent variable $\bar{z} = l - z$, which maps the second half of the structure into the first half. Using the result of S_1, we deduce that

$$S_2 = \begin{bmatrix} (1 - d\tau_0)e^{-2ikl} & \tau_0 \\ \tau_0 & (1 - \tau_0/d)e^{2ikl} \end{bmatrix}, \tag{2.25}$$

where e^{2ikl} and e^{-2ikl} take into account the physical location of the channel at $z = l$. Therefore, the amplitudes of outgoing waves T_{00} and A_0 are related to the amplitudes of the incoming waves B_0 by S_2, as follows.

$$\begin{bmatrix} T_{00} \\ A_0 \end{bmatrix} = S_2 \begin{bmatrix} 0 \\ B_0 \end{bmatrix} \tag{2.26}$$

One of the input wave amplitude is 0 because in the region $z > l$, there is no incident wave to the slab problem.

To determine a scattering matrix of the slab structure, we first solve for A_0 in terms of B_0 from equation (2.21). Then we substitute A_0 in equation (2.26) and find B_0. The transmission coefficient T_{00} and the reflection coefficient R_{00} are determined from (2.21) and (2.26), respectively. These results are summarized as

$$\begin{bmatrix} R_{00} \\ T_{00} \end{bmatrix} = S \begin{bmatrix} 1 \\ 0 \end{bmatrix}, \tag{2.27}$$

where

$$S = \begin{bmatrix} (1 - d\tau_0) + \frac{\tau_0^2(1-\tau_0/d)e^{2ikl}}{M} & \frac{\tau_0^2}{M} \\ \frac{\tau_0^2}{M} & (1 - d\tau_0)e^{-2ikl} + \frac{\tau_0^2(1-\tau_0/d)}{M} \end{bmatrix}, \tag{2.28}$$

and $M = 1 - (1 - \tau_0/d)^2 e^{2ikl}$. The scattering matrix S represents the slab structure and connects the reflected and transmitted waves of the lowest mode to the incident wave, if k is chosen such that only one mode propagates. In the matrix S, there is only one parameter τ_0 which is the transmission coefficient of the first auxiliary problem. Therefore, the reflection and transmission coefficients R_{00} and T_{00} are found in terms of τ_0. As in the two-dimensional case addressed in [20], the solution of the three-dimensional problem is dependent on only one parameter τ_0. Coefficient τ_0 is a function of a real number η (equation (2.24)). In Chapter 3, we will approximate η numerically and find the transmission properties of the slab structure.

CHAPTER 3

NUMERICAL RESULTS AND TRANSPARENCY

In Chapter 2, the scattering matrix S for the slab structure was derived. Expressions for the transmitted and the reflected coefficients were obtained using the scattering matrix S. They are

$$T_{00} = \frac{\tau_0^2}{1-(1-\tau_0/d)^2 e^{2ikl}} \tag{3.1a}$$

$$R_{00} = (1-d\tau_0) + \frac{\tau_0^2(1-\tau_0/d)e^{2ikl}}{1-(1-\tau_0/d)^2 e^{2ikl}}. \tag{3.1b}$$

These two coefficients are functions of only one parameter τ_0 from the first auxiliary problem. Since the first auxiliary problem cannot be solved analytically, a numerical approximation to the parameter τ_0 will be found using the characteristic size d of the hole. Once the parameter τ_0 is found, we are able to discuss the behavior of the transmitted and the reflected waves of the slab structure.

This chapter is organized as follows. In Section 3.1, using an appropriate Green's function we deduce an integral representation for the solution $u_1(x, y, z)$ in the region $z < 0$. Then, by substituting the modal solutions in the integral equation and by using the orthonormality of the eigenfunctions, we obtain an infinite system of algebraic equations with unknowns τ_p $(p \geq 0)$. An expression for τ_0 is found explicitly through these equations. It is observed that τ_0 follows the same constraint as the analytic solution in Chapter 2. In Section 3.2, each coefficient Z_{qp} in the infinite system of algebraic equations is evaluated for circular holes and rectangular holes, respectively. By employing the small parameter d, τ_0 is found approximately. In Section 3.3, the transmission and the reflection coefficients are plotted as functions of k or l for different cases. This is followed by a detailed discussion of the frequency selecting properties of the structure. Lastly, the conclusion is included in Section 3.4.

3.1 Numerical Expression of τ_0

The diagram of the first auxiliary problem is shown in Figure 2.3. The wave is normally incident upon the channel. A part of the incident wave is reflected and the remaining is transmitted. The modal solution (equation (2.12)) was derived in Chapter 2. In order to derive equations to solve for τ_0, we introduce a Green's function. This Green's function will be used to deduce an integral representation of the solution to the first auxiliary problem. The Green's function satisfies

$$\nabla^2 G + k^2 G = \delta(\vec{x} - \vec{x}') \qquad z' < 0, \tag{3.2a}$$

$$\frac{\partial G}{\partial z} = 0 \qquad when\ z = 0, \tag{3.2b}$$

and is periodic in both x and y directions. This function G is solved explicitly as

$$G(\vec{x}|\vec{x}') = \begin{cases} \sum_{-\infty}^{\infty}\sum_{-\infty}^{\infty} \frac{\cos\beta_{mn}z'}{i\beta_{mn}} e^{2m\pi i(x-x')/a} e^{2n\pi i(y-y')/b} e^{-ikz}, & -\infty < z < z' \\ \sum_{-\infty}^{\infty}\sum_{-\infty}^{\infty} \frac{\cos\beta_{mn}z}{i\beta_{mn}} e^{2m\pi i(x-x')/a} e^{2n\pi i(y-y')/b} e^{-ikz'}, & z' < z < 0. \end{cases} \tag{3.3}$$

Since u_1 satisfies the Helmholtz equation, it follows from (3.2a) that

$$\nabla \cdot (u_1 \nabla G - G \nabla u_1) = u_1 \delta(\vec{x} - \vec{x}'). \tag{3.4}$$

Integrating equation (3.4) over the region R_c, ($-\infty < z < 0$, $|x| < a/2$ and $|y| < b/2$) and applying the divergence theorem yields,

$$u_1(x', y', z') = \iint (u_1 G_n - G u_{1n}) ds, \tag{3.5}$$

where the surface integral is over the six faces of the cube R_c. The surface integrals over the four sides vanish because of periodic boundary conditions. The surface integrals over the plane $z = -\infty$ and $z = 0^-$ remain. At $z = -\infty$, since all the higher order modes are damped, G behaves like $\cos(kz')e^{-ikz}/ik$ and u_1 behaves like $e^{ikz}\psi_{00} + r_{00}e^{-ikz}\psi_{00}$. The surface integration over the plane $z = -\infty$ gives

$2\cos(kz')\psi_{00}$. Therefore,

$$u_1(x,y,z) = (2\cos kz)\psi_{00} - \iint_{z=0^-} G(x',y',0^-|x,y,z)\frac{\partial u_1}{\partial z}(x',y',0^-)ds'. \qquad (3.6)$$

On the surface $z = 0^-$, the derivative $\partial u_1/\partial z$ vanishes outside the surface of the hole. Thus, the double integral on the right hand side of equation (3.6) is over only the surface of the hole. This implies that

$$u_1(x,y,z) = (2\cos kz)\psi_{00} - \iint_H G(x',y',0^-|x,y,z)\frac{\partial u_1}{\partial z}(x',y',0^-)ds'. \qquad (3.7)$$

Equation (3.7) is an integral representation of u_1 in the region $z < 0$. The first term in equation (3.7) is the sum of the normally incident wave e^{ikz} and its rigid reflection e^{-ikz}. It is the field that would occur if no holes were present. In the second term, the integration is over the surface of the hole. Since the hole is small, the second term can be considered as a perturbation to the field in the region $z < 0$ due to the existence of small holes in the structure.

Setting $z = 0^-$ in equation (3.7), we obtain the field at the interface $z = 0$,

$$u_1(x,y,0^-) = 2\psi_{00} - \iint_H G(x',y',0^-|x,y,0^-)\frac{\partial u_1}{\partial z}(x',y',0^-)ds'. \qquad (3.8)$$

Since both u_1 and $\partial u_1/\partial z$ are continuous across $z = 0$ on the surface of the hole, we let $z = 0^+$ and substitute from equation (2.12b) to get

$$\sum_{p=0}^{\infty} \tau_p\varphi_p(x,y) = 2\psi_{00} - \iint_H G(x',y',0|x,y,0)\sum_{p=0}^{\infty} ik_p\tau_p\varphi_p(x',y')ds'. \qquad (3.9)$$

Multiplying both sides of the equation by φ_q, integrating the resulting equation over the surface of the hole and using the orthonormality of the eigenfunctions yields

$$\tau_q = 2d\delta_{q0} - i\sum_{p=0}^{\infty} k_p\tau_p Z_{qp} \qquad q = 0,1,2,\cdots, \qquad (3.10)$$

where

$$Z_{qp} = \iint_H \iint_H G(x',y',0|x,y,0)\varphi_p(x',y')\varphi_q(x,y)ds'ds \qquad (3.11)$$

and δ_{q0} is the Kronecker delta function. When d is small, there is only one mode propagates in the hole channel, which implies that k_p is imaginary for all $p \geq 1$ ((2.7)). Hence k_p can be written as $i|k_p|$. Substituting $i|k_p|$ in the equations for τ_q gives

$$\tau_0 = 2d - ik\tau_0 Z_{00} + \sum_{p=1}^{\infty} |k_p| Z_{0p}\tau_p, \tag{3.12a}$$

$$\tau_q = -ik\tau_0 Z_{q0} + \sum_{p=1}^{\infty} |k_p| Z_{qp}\tau_p \qquad q = 1, 2, \cdots . \tag{3.12b}$$

The equations in (3.12) form an infinite system of algebraic equations with unknowns τ_p. The quantities Z_{qp} are defined in (3.11). If the eigenfunctions φ_p are known, Z_{qp} can be found either analytically or numerically for each p and q. Therefore, each τ_p can be solved for approximately by truncating the infinite system.

Before truncating the algebraic system (3.12), we simplify it further, so as to find an explicit representation for τ_0 which is comparable to (2.24). Setting $\alpha_q = \tau_q/(-ik\tau_0)$ for $q \geq 1$ and substituting α_q in (3.12b) gives

$$\alpha_q = Z_{q0} + \sum_{p=1}^{\infty} |k_p| Z_{qp}\alpha_p \qquad q = 1, 2, \cdots . \tag{3.13}$$

The same change of variable applied to (3.12a) yields

$$\tau_0 = \frac{2d}{1 + ikZ_{00} + ik\sum_{p=1}^{\infty} |k_p| Z_{0p}\alpha_p}. \tag{3.14}$$

Thus, τ_0 can be found explicitly, provided α_q are known. Values for α_q are determined using equation (3.13).

Expressions of quantities Z_{qp} depend on the shape of the hole. However, the first eigenfunction $\varphi_0 = 1/d$ is the same for all shapes. Therefore, we can determine

the first term in Z_{00}. From equation (3.11), Z_{00} is defined as

$$\begin{aligned} Z_{00} &= \iint_H \iint_H G(x', y', 0|x, y, 0)\varphi_0^2 ds' ds \\ &= \iint_H \iint_H G(x', y', 0|x, y, 0)\frac{1}{d^2} ds ds'. \end{aligned} \tag{3.15}$$

The Green's function G in equation (3.3) can be rewritten as

$$\begin{aligned} G(x', y', 0|x, y, 0) = \frac{1}{ik} &+ \sum_{n=1}^{\infty} \frac{2}{i\beta_{0n}} \cos\frac{2n\pi(y-y')}{b} + \sum_{m=1}^{\infty} \frac{2}{i\beta_{m0}} \cos\frac{2m\pi(x-x')}{a} \\ &+ \sum_{m=1}^{\infty}\sum_{n=1}^{\infty} \frac{4}{i\beta_{mn}} \cos\frac{2m\pi(x-x')}{a} \cos\frac{2n\pi(y-y')}{b}. \end{aligned} \tag{3.16}$$

Substituting Green's function in the expression for Z_{00} and integrating the first term, implies that the first term is $\frac{d^2}{ik}$ for any shape of the hole. Hence, Z_{00} can be rewritten as,

$$Z_{00} = \frac{d^2}{ik} + \tilde{Z}_{00}. \tag{3.17}$$

Substitute Z_{00} thus found, in the expression for τ_0 in equation (3.14) gives,

$$\tau_0 = \frac{2d}{1 + d^2 + ik(\tilde{Z}_{00} + \sum_{p=1}^{\infty} |k_p| Z_{0p}\alpha_p)}. \tag{3.18}$$

Equation (3.18) shows that the approximation for τ_0 satisfies the same constraint as the one derived in the Chapter 2, described in equation (2.24), with

$$\eta = k(\tilde{Z}_{00} + \sum_{p=1}^{\infty} |k_p| Z_{0p}\alpha_p). \tag{3.19}$$

Having found τ_0 explicitly, we now continue with truncating the system in equation (3.13), in order to solve for α_q. Truncation inevitably introduces errors. However, no matter how much error is introduced, the approximation for τ_0 always lies on the circle defined by equation (2.23). This expression is valid regardless of the shape of the hole.

Since the transmission coefficient T_{00} is a function depending only on the parameter τ_0, and τ_0 cannot be found explicitly if the hole shape is not specified. In the following sections, we will discuss the transmission properties of the slab structure for holes with two kinds of shapes, namely, circular and rectangular.

3.2 An Approximation to τ_0

In the expression for τ_0 in equation (3.18), the real number η needs to be computed. Since η is a function of Z_{qp} and α_q (equation (3.19)), we shall first evaluate the parameters Z_{qp} and α_q in order to determine η and hence determine τ_0. In this section, τ_0 is determined for circular holes and rectangular holes.

3.2.1 Results of Circular Holes

If the hole is circular with dimensional radius R, then the characteristic size of the hole is $D = \sqrt{\pi}R$. After nondimesionalization, we obtain that $d = \sqrt{\pi}r$. Therefore, the eigenfunctions corresponding to the circular hole can be easily obtained as follows,

$$\begin{aligned} \varphi_0 &= \frac{1}{d}, \\ \varphi_p(r) &= \frac{1}{d}\frac{J_0(\lambda_p r)}{J_0(\lambda_p d/\sqrt{\pi})} \qquad p = 1, 2, \cdots, \end{aligned} \tag{3.20}$$

where J_0 is the zeroth order Bessel function. The corresponding eigenvalues are found to be $\lambda_p = j_{1p}\sqrt{\pi}/d$, where j_{1p} is the p^{th} root of the first order Bessel function. As mentioned before, for $d << 1$, propagation constants

$$k_p = \sqrt{k^2 - \lambda_p^2} \tag{3.21}$$

in the channel and can be approximated by

$$k_p \approx i j_{1p}\sqrt{\pi}/d \qquad p \geq 1. \tag{3.22}$$

Now, the quantities Z_{qp} can be found explicitly using the explicit expressions of the Green's functions and the eigenfunctions. The integral in equation (3.11) is computed by interchanging the order of integral and the summation (see Appendix D). The results thus obtained are described below.

$$\begin{aligned} Z_{00} &= \frac{d^2}{ik} + d^2 \left(\sum_{m=1}^{\infty} \frac{-8}{|\beta_{m0}|} \frac{J_1^2(\mu_1)}{\mu_1^2} + \sum_{n=1}^{\infty} \frac{-8}{|\beta_{0n}|} \frac{J_1^2(\mu_2)}{\mu_2^2} + \sum_{m=1}^{\infty}\sum_{n=1}^{\infty} \frac{-16}{|\beta_{mn}|} \frac{J_1^2(\mu_3)}{\mu_3^2} \right) \\ &\equiv \frac{d^2}{ik} + d^2 S_{00}, \end{aligned} \tag{3.23}$$

$$\begin{aligned} Z_{qp} &= d^2 \sum_{m=1}^{\infty} \frac{-8}{|\beta_{m0}|} \frac{\mu_1^2 J_1^2(\mu_1)}{(\mu_1^2 - j_{1p})(\mu_1^2 - j_{1q})} + d^2 \sum_{n=1}^{\infty} \frac{-8}{|\beta_{0n}|} \frac{\mu_2^2 J_1^2(\mu_2)}{(\mu_2^2 - j_{1p})(\mu_2^2 - j_{1q})} \\ &\quad + d^2 \sum_{m=1}^{\infty}\sum_{n=1}^{\infty} \frac{-16}{|\beta_{mn}|} \frac{\mu_3^2 J_1^2(\mu_3)}{(\mu_3^2 - j_{1p})(\mu_3^2 - j_{1q})} \qquad (3.24) \\ &\equiv d^2 S_{qp} \qquad p^2 + q^2 \geq 1, \end{aligned}$$

where μ_1, μ_2 and μ_3 are defined as

$$\mu_1 = 2m\sqrt{\pi}d/a, \tag{3.25a}$$

$$\mu_2 = 2n\sqrt{\pi}d/b, \tag{3.25b}$$

$$\mu_3 = \sqrt{(2m\sqrt{\pi}d/a)^2 + (2n\sqrt{\pi}d/b)^2}. \tag{3.25c}$$

We observe that in equation (3.24), the quantities Z_{qp} are symmetric and hence $S_{pq} = S_{qp}$. Substituting the new notation in equations (3.13) and (3.18), respectively, gives,

$$\alpha_q = d^2 S_{q0} + d^2 \sum_{p=1}^{\infty} |k_p| S_{qp} \alpha_p \qquad q = 1, 2, \cdots \tag{3.26}$$

and

$$\tau_0 = \frac{2d}{1 + d^2 + id^2 \left(kS_{00} + k \sum_{p=1}^{\infty} |k_p| S_{0p} \alpha_p \right)}. \tag{3.27}$$

The infinite system of equations (3.26) cannot be solved unless the system is truncated at $p = q = N$. Truncation yields an approximation for α_q as the solution

of equation (3.28),

$$\hat{\alpha}_q = d^2 S_{q0} + \sum_{p=1}^{N} |k_p| \hat{\alpha}_p \cdot d^2 S_{qp}, \tag{3.28}$$

where $\hat{}$ (the hat) denotes an approximate value. Since only one mode propagates in the channel, N is relatively small [20]. We recall the definition of k_p and observe that $|k_p| \sim j_{1p}\sqrt{\pi}/d$ for $p \geq 1$ and d approaches 0. Hence, equation (3.28) can be approximated by,

$$\hat{\alpha}_q = d^2 S_{q0} + d \sum_{p=1}^{N} j_{1p}\sqrt{\pi} S_{qp} \hat{\alpha}_p. \tag{3.29}$$

We will now employ the small parameter d to solve equation (3.29) approximately. Before doing that, we first check the order of S_{qp} as d approaches 0. Figures 3.1, 3.2 and 3.3 show this behavior for S_{00}, S_{0p} and S_{qp}, respectively. In Figure 3.1, we

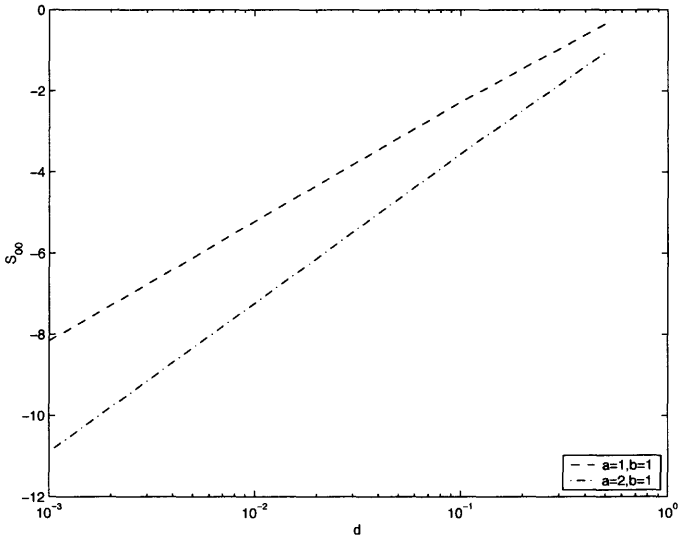

Figure 3.1 The behavior of S_{00} for small value of d.

observe that, as d approaches 0, S_{00} decreases and behaves like $ln(d)$. In Figure 3.2 and Figure 3.3 we observe that S_{0p} and S_{qp} are very small compared to S_{00}. In particular as d approaches 0, S_{0p} become a constant and S_{qp} approach 0 rapidly. Thus, both S_{0p} and S_{qp} are order one quantities as d approaches 0.

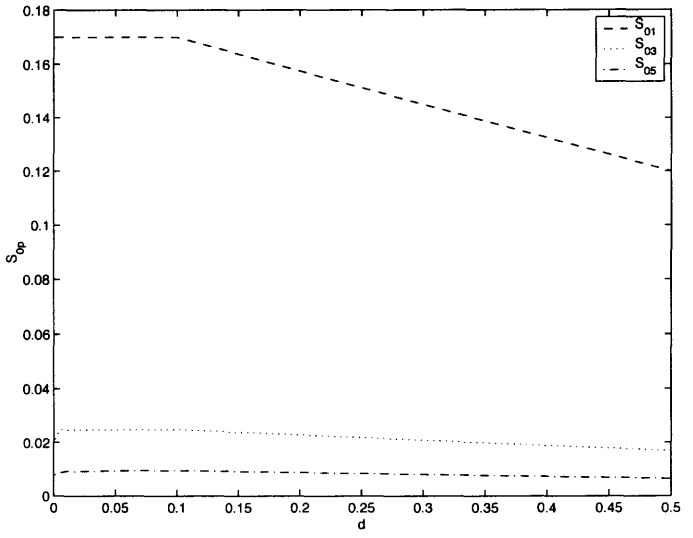

Figure 3.2 The behavior of S_{0p} for small value of d.

Using the fact that both S_{0p}, S_{qp} are of $O(1)$ for small value of d and the fact that $d << 1$, equation (3.28) is solved iteratively and yields

$$\hat{\alpha}_q = d^2 S_{q0} + O(d^3), \qquad 1 \leq q \leq N. \tag{3.30}$$

Substituting $\hat{\alpha}_q$ from above and truncating the infinite series at $p = N$ in the expression for η (equation (3.19)) gives the approximation,

$$\hat{\eta} \approx d^2 k\{S_{00} + d\sum_{p=1}^{N} j_{1p}\sqrt{\pi}S_{0p}^2\}. \tag{3.31}$$

As d approaches 0, the second term in curly brackets is much smaller than the first term. This is because as d approaches 0, S_{0p} is of $O(1)$ and S_{00} is of $O(\ln d)$. Therefore, neglecting the second term gives an approximation of η,

$$\hat{\eta} \approx d^2 k S_{00}. \tag{3.32}$$

Thus, the numerical approximation of τ_0 for the small value of d is

$$\hat{\tau_0} \approx \frac{2d}{1 + d^2 + id^2 k S_{00}}. \tag{3.33}$$

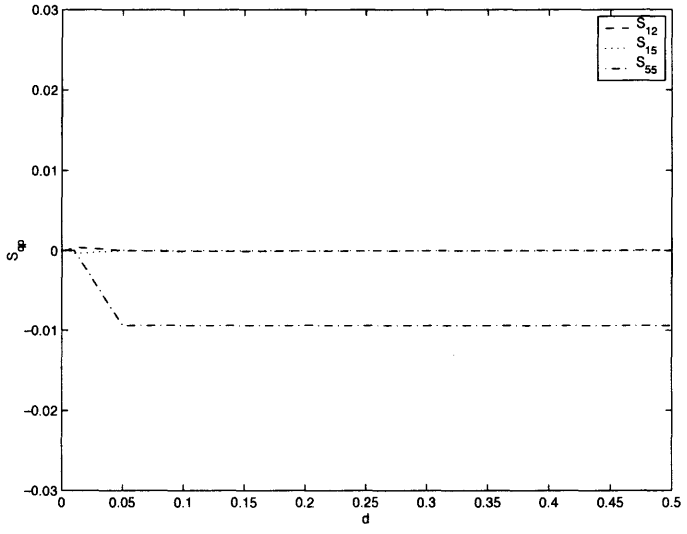

Figure 3.3 The behavior of S_{qp} for small value of d.

We reiterate that, the numerical approximation of τ_0 in equation (3.33) follows the same constraint as in equation (2.24).

3.2.2 Results of Rectangular Holes

Due to its symmetry, a rectangular hole allows the corresponding eigenvalues and eigenfunctions to be stated explicitly. We assume that rectangular holes are placed symmetrically about the $x-$ and the $y-$ axes. The length and the width of the hole are D_1 and D_2, respectively. The corresponding dimensionless length is $d_1 = D_1/\sqrt{AB} << 1$ and the dimensionless width is $d_2 = D_2/\sqrt{AB} << 1$. Hence, the characteristic size of the rectangular hole is, $d = \sqrt{d_1 d_2}$. The solution in the channel in terms of eigenfunctions is written as,

$$u(x,y,z) = \sum_{p=0}^{\infty}\sum_{q=0}^{\infty}(A_{pq}e^{-ik_{pq}z} + B_{pq}e^{ik_{pq}z})\phi_{pq}(x,y) \qquad 0 < z < l \tag{3.34}$$

where

$$\phi_{00} = \frac{1}{d}, \tag{3.35a}$$

$$\phi_{p0} = \frac{\sqrt{2}}{d} \cos \frac{2p\pi x}{d_1}, \qquad \phi_{0q} = \frac{\sqrt{2}}{d} \cos \frac{2q\pi y}{d_2}, \tag{3.35b}$$

$$\phi_{pq} = \frac{1}{d} \cos \frac{2p\pi x}{d_1} \cos \frac{2q\pi y}{d_2}, \qquad p, q = 1, 2, 3 \cdots \tag{3.35c}$$

and

$$k_{pq} = \sqrt{k^2 - \left(\frac{2p\pi}{d_1}\right)^2 - \left(\frac{2q\pi}{d_2}\right)^2} \qquad p, q = 0, 1, 2 \cdots . \tag{3.36}$$

The eigenvalues and the eigenfunctions corresponding to the rectangular hole have two indices p and q instead of one as in the circular case. However, since both d_1 and d_2 are very small, k_{pq} can still be approximated by

$$k_{pq} \approx i\sqrt{\left(\frac{2p\pi}{d_1}\right)^2 + \left(\frac{2q\pi}{d_2}\right)^2} \qquad p^2 + q^2 > 0 \tag{3.37}$$

which shows that the corresponding modes are highly damped in the channel.

For the rectangular hole, we still have the infinite system of equations for the transmission coefficients τ_{pq}. The only difference is that we have two indices now instead of one. Therefore, we write down the representation for τ_{00} as,

$$\tau_{00} = \frac{2d}{1 + ikZ_{0000} + ik \sum\sum |k_{pq}| \alpha_{pq} Z_{00pq}} \tag{3.38}$$

where the double summation is for all p, q such that $p^2 + q^2 > 0$. Here α_{pq} are the solutions of

$$\alpha_{pq} = Z_{pq00} + \sum\sum |k_{pq}| Z_{pqrs} \alpha_{rs} \qquad p^2 + q^2 > 0, \tag{3.39}$$

where the double summation is for all r, s such that $r^2 + s^2 > 0$. We compute Z_{pqrs} explicitly and the results are

$$\begin{aligned} Z_{pqrs} &= \frac{d^2}{ik}\delta_{p0}\delta_{q0}\delta_{r0}\delta_{s0} + d^2 \sum_{m=1}^{\infty} \frac{-2}{|\beta_{m0}|}(\sqrt{2})^N f(\frac{m\pi d_1}{a}, p, r)\delta_{q0}\delta_{s0} \\ &+ d^2 \sum_{n=1}^{\infty} \frac{-2}{|\beta_{0n}|}(\sqrt{2})^N f(\frac{n\pi d_2}{b}, q, s)\delta_{p0}\delta_{r0} \\ &+ d^2 \sum_{m=1}^{\infty}\sum_{n=1}^{\infty} \frac{-4}{|\beta_{mn}|}(\sqrt{2})^N f(\frac{m\pi d_1}{a}, p, r) f(\frac{n\pi d_2}{a}, q, s) \\ &\equiv \frac{d^2}{ik} + d^2 S_{pqrs} \qquad\qquad p, q, r, s = 0, 1, 2 \cdots, \end{aligned} \tag{3.40}$$

where the function f is defined as

$$f(t, n_1, n_2) \equiv (-1)^{n_1+n_2} \frac{t^2(\sin t)^2}{(t^2 - (n_1\pi)^2)((t^2 - (n_2\pi)^2)} \tag{3.41}$$

with n_1 and n_2 being integers. The power N in $(\sqrt{2})^N$ is the number of nonzero terms in the sequence $\{p, q, r, s\}$, so that $0 \leq N \leq 4$. The propagation constants β_{mn} are defined in equation (2.4).

Substituting from equation (3.40) in equations (3.38) and (3.39) yields

$$\tau_{00} = \frac{2d}{1 + d^2 + ikd^2(S_{0000} + \sum\sum |k_{pq}|\alpha_{pq}S_{00pq})}, \tag{3.42}$$

and

$$\alpha_{pq} = d^2 S_{pq00} + d^2 \sum\sum |k_{pq}| S_{pqrs}\alpha_{rs} \qquad p^2 + q^2 > 0, \tag{3.43}$$

respectively. S_{pqrs} are order one parameters for p, q, r, s such that $p^2+q^2+r^2+s^2 > 0$. As d approaches 0, if S_{0000} is the dominant term, then the approximation used for circular holes can be used for rectangular holes as well.

The behaviors of S_{0000} are shown in Figure 3.4. For fixed d_1, as d_2 approaches 0, S_{0000} lies between $\ln d$ and $1/d$. In Figures 3.5 and 3.6, functions S_{pqrs} approach constants for small value of d. Although, we cannot graph functions S_{pqrs} for all

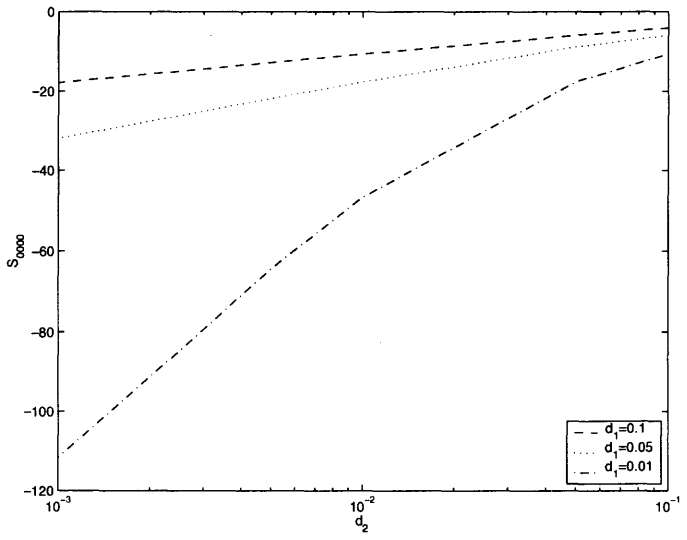

Figure 3.4 The behavior of S_{0000} as d_1 and d_2 approach 0 for $a = b = 1$.

values of p, q r and s, their behavior is the same for small value of d. As the indices p, q, r and s become larger and as d approaches 0, functions S_{pqrs} approach smaller constants. This is observed from Figure 3.5.

Figures 3.4, 3.5 and 3.6 demonstrate the dominant behavior of S_{0000} for small value of d, and hence an approximation for τ_{00} can be written as

$$\hat{\tau}_{00} = \frac{2d}{1 + d^2 + ikd^2 S_{0000}}. \tag{3.44}$$

3.3 Transmission Properties of the Perforated Slab

Through the analysis in Sections 3.1 and 3.2, we obtained an approximation of τ_0 for small values of d. We are now ready to approximate T_{00} numerically. Function T_{00} is found to be

$$T_{00} = \frac{\tau_0^2}{1 - (1 - \tau_0/d)^2 e^{2ikl}}. \tag{3.45}$$

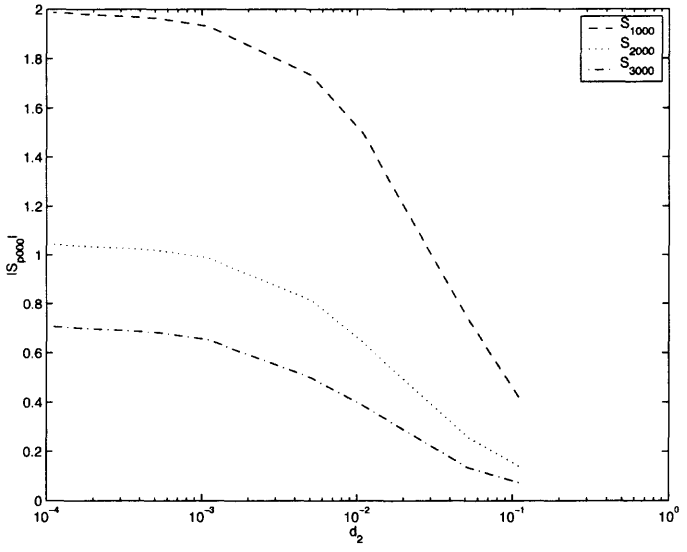

Figure 3.5 The behavior of S_{p000} as d_2 approaches 0 for $d_1 = 0.051$ and $a = b = 1$.

Substituting the approximation $\hat{\tau}_0$ from equation (3.33), we find that,

$$\begin{aligned} |\hat{T}_{00}| &= \frac{2d^2}{\sqrt{(2d^2\nu_1)^2 + \nu_2^2}} \\ \nu_1 &= d^2 k S_{00} \sin kl + \cos kl \\ \nu_2 &= (1 + d^4 - d^4 k^2 S_{00}^2) \sin kl - 2d^2 k S_{00} \cos kl. \end{aligned} \tag{3.46}$$

The result obtained in equation (3.46) is for circular holes. The result is the same for the rectangular holes except that S_{00} is replaced by S_{0000}.

We first discuss the behavior of circular holes. If kl is such that ν_2 is an order one quantity, then T_{00} is $O(d^2)$, which is very small since d is small. In this case, there is not much transmission into the region $z > l$. This agrees with our intuition, because when the holes are small, most of the acoustic waves reflect back into $z < 0$ and very little transmits. However, there exist values for kl such that $\nu_2 = 0$, that is,

$$\tan kl = \frac{2d^2 k S_{00}}{1 + d^4(1 - k^2 S_{00})}, \tag{3.47}$$

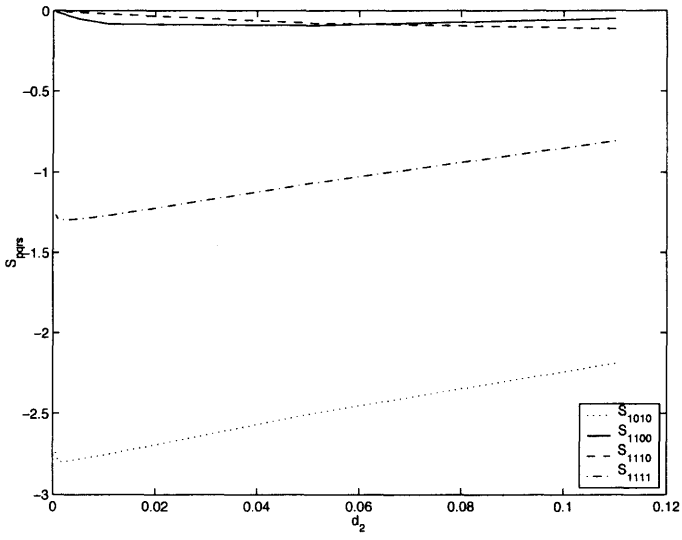

Figure 3.6 The behavior of S_{pqrs} as d_2 approaches 0 for $d_1 = 0.051$ and $a = b = 1$.

then in this case,

$$|\hat{T}_{00}| = 1/\nu_1 = \frac{1/\cos kl}{1 + d^2 k S_{00} \tan kl}. \tag{3.48}$$

Using the fact that $d << 1$, solution of equation (3.47) can be approximated as,

$$kl \approx M\pi + 2d^2 k S_{00} + O((d^2 S_{00})^3) \tag{3.49}$$

where M is any positive integer. Using the values of kl thus obtained in equation (3.48), we deduce,

$$|\hat{T}_{00}| \approx 1 - O((d^2 S_{00})^4). \tag{3.50}$$

Therefore, for these values of kl, the slab is almost transparent. That is, for a fixed frequency k, the thickness l of the slab determines its transmission properties.

Figure 3.7 is plotted using equation (3.46). It shows that, T_{00} is almost 0 for all thicknesses l of the slab except at $l \approx 1, 2, 3 \cdots$, where $T_{00} \approx 1$. Actually, the peaks occurs just to the left of these integers. The difference is 0.001, which agrees with our approximation for l, since for $S_{00} = -5.2$ and $d = 0.01$, $2d^2 S_{00} \approx 0.001$.

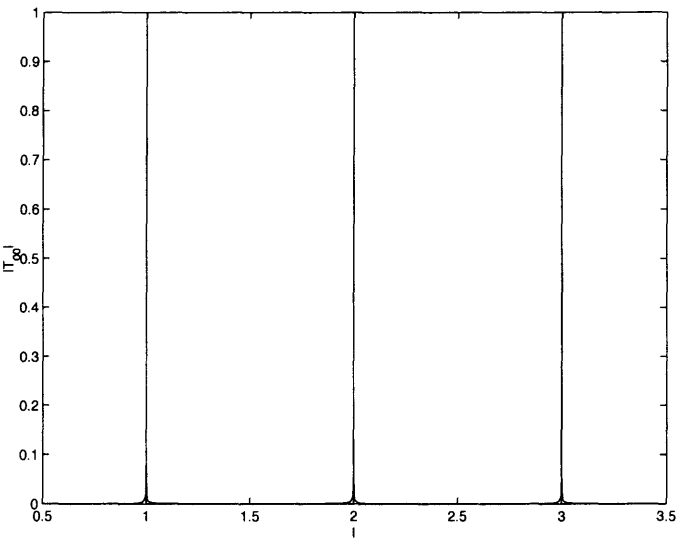

Figure 3.7 Transmission coefficient T_{00} versus the thickness of the slab l for $d = 0.01$, $k = \pi$ and $a = b = 1$.

This agreement is also seen in Figure 3.8, where $S_{00} = -2.28$ and $d = 0.1$. In this figure, the peaks appear some distance to the left of $l = 1, 2, 3 \cdots$, and the difference is 0.0456, which equals $2d^2 S_{00}$. Also, Figures 3.7 and 3.8 verify that, away from the peaks, the values of T_{00} are $O(d^2)$.

Similarly, we can fix the thickness of the slab and solve equation (3.47) for k to find the frequency at which the structure is transparent. Since S_{00} is also a function of k, it is not easy to find an explicit expression. However, it is easy to check numerically that, when $k < 2\pi/a$, S_{00} is not a sensitive function of k. Thus from equation (3.49), k can be approximated as,

$$k = \frac{M\pi}{l - 2d^2 S_{00}}. \tag{3.51}$$

For these k's, $T_{00} \approx 1$. The behaviors of $|T_{00}|$ as a function of k are illustrated in Figures 3.9 and 3.10, where $l = 1$ and 2, respectively. The peaks occur just at the position estimated by equation (3.51). The number of peaks increases as l increases when the upper limit of k is fixed.

It is clear from these figures that the perforated rigid slab as considered in

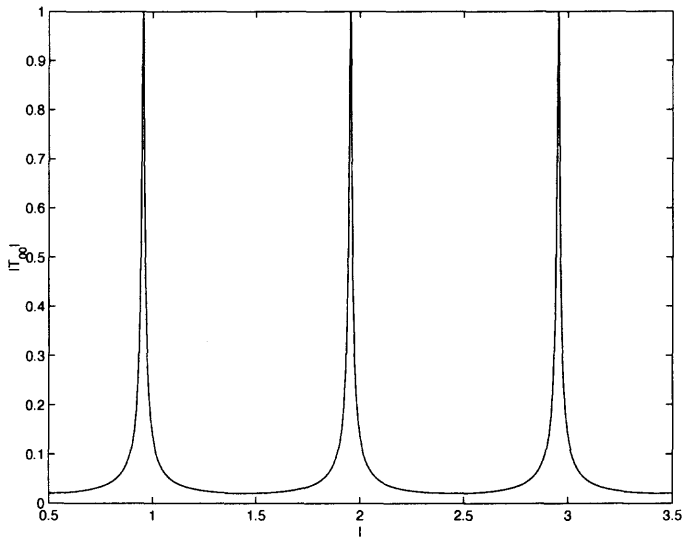

Figure 3.8 Transmission coefficient T_{00} versus the thickness of the slab l for $d = 0.1$, $k = \pi$ and $a = b = 1$.

the problem, behaves like a narrow band filter. For certain frequencies, energy is transmitted almost 100%; for other frequency bands, almost all the energy is reflected. Also, the width of the passing band depends on the dimensionless radius of the holes. If dimension is reintroduced, the width of the passing band depends on the porosity of the rigid slab.

For rectangular holes, we have the same results as those for circular holes. In Figure 3.11, the reflection coefficient R_{00} is shown for different values of l for a fixed k. Most of the waves are reflected when the hole is small. However, for some values of kl the waves are completely transmitted.

3.4 Conclusion

In Chapters 2 and 3, we analyzed the problem of a normally incident acoustic wave propagation through a periodically perforated rigid slab. We assumed that the characteristic size of a hole is much smaller than the spacing of the holes, while the incident wave length is of the same order as the spacing of the holes. We also restricted the range of the incident wave frequency such that there is only one mode

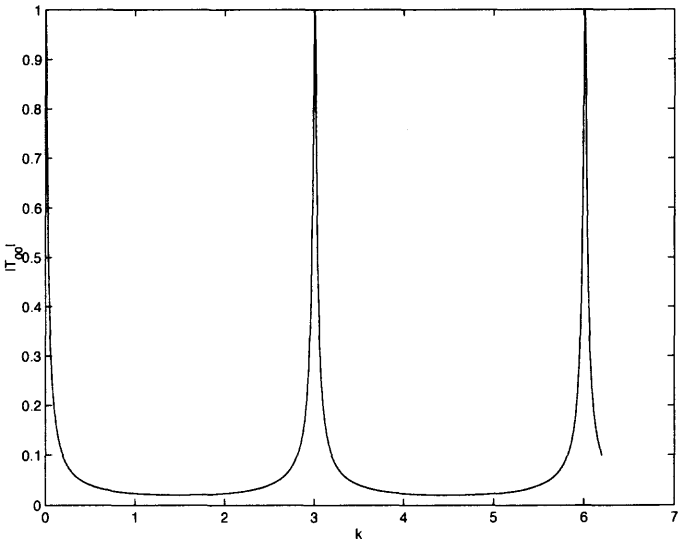

Figure 3.9 Transmission coefficient T_{00} versus wavenumber k for $d = 0.1$, $l = 1$ and $a = b = 1$.

propagates both outside the slab and inside the holes. The length of the slab in our problem is long enough so that all the evanescent modes are negligible in the middle of the hole channel. Under these assumptions, we considered two auxiliary problems. Both of the auxiliary problems are of the same structures as the slab except that they are infinitely long. In the first auxiliary problem, the wave is incident from the air; in the second auxiliary problem, the wave is incident from the hole. The relationship of the transmission and the reflection coefficients of the two problems were discussed in detail. The linear combination of the two auxiliary problems gave a scattering matrix S for the original structure. Through this matrix S, the transmission coefficient T_{00} and the reflection coefficient R_{00} of the slab were found explicitly. It turned out that, for arbitrary shaped holes, coefficients T_{00} and R_{00} depend only on one parameter τ_0 which is the transmission coefficient of the first auxiliary problem. This τ_0 was found lying on a circle of a complex plane.

The numerical value of τ_0 was found for both circular and rectangular holes. Specifically, an infinite system of algebraic equations was derived from the integral

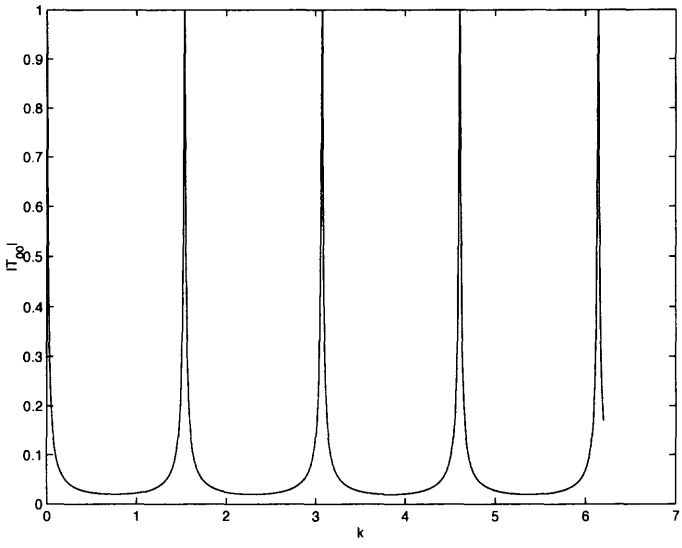

Figure 3.10 Transmission coefficient T_{00} versus wavenumber k for $d = 0.1$, $l = 2$ and $a = b = 1$.

representation of the solution of the first auxiliary problem. Coefficient τ_0 was solved explicitly from these algebraic equations. By using the fact that the hole size is very small comparing to the spacing of the holes, τ_0 was obtained numerically. The plots of $|T_{00}|$ were given for both circular and rectangular holes. The plots showed that for fixed thickness of the slab, the function $|T_{00}|$ is $O(d^2)$ quantities except at certain frequencies, at which the wave can transmit almost completely. On the other hand, if the frequency of the incident wave is fixed, by adjusting the thickness of the slab, we can have either completely transmitted wave or completely reflected wave. This frequency selection properties of the structure make itself useful in constructing filters or resonators.

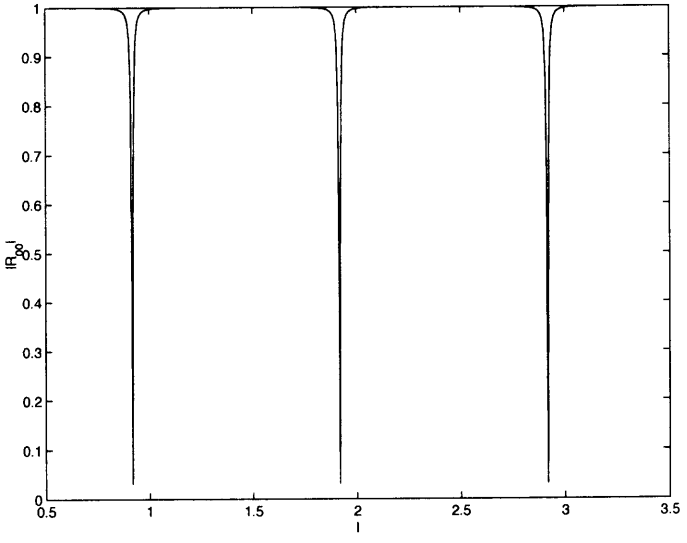

Figure 3.11 Reflection coefficient R_{00} versus the thickness of the slab l for $k = \pi$, $d_1 = d_2 = 0.1$ and $a = b = 1$.

CHAPTER 4

PERTURBATION ANALYSIS ON MICROSTRIP

4.1 Introduction

In the 1950's, strip lines were introduced as substitutions for two-wire lines, to adapt with the planar geometry of printed circuits [5]. Subsequently, these transmission lines have been extensively used in microwave and millimeter wave integrated circuits. They are used to build components and devices in circuits such as filters, couplers, antennae and so on, and they are also used to connect varieties of networks. These transmission lines have many advantages in microwave printed circuits: They are small, simple, reliable and inexpensive with good electrical characteristics [12]. A typical geometry of a microstrip transmission line is shown in Figure 4.1: Above the metal ground plane, there is a dielectric substrate, on the top of which is a thin metal strip.

There are many papers on the electrical characteristics of microstrip transmis-

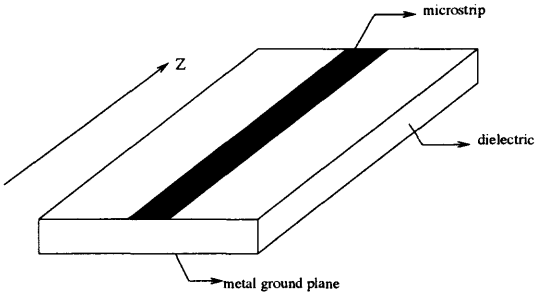

Figure 4.1 A microstrip transmission line.

sion lines. One reason is because of its usefulness in printed circuits, so that a full understanding of its behavior is very important; another reason is that there is no exact solution of Maxwell equations for this geometry. Therefore, it is a very rich problem to apply different techniques of mathematics. Among these papers, the

dispersive properties of microstrip are especially interesting and important because dispersion is one of the disadvantages of this transmission line.

A transmission line is dispersive means that the phase velocity of a signal is a function of frequency. Microstrip belongs to this category because in a microstrip transmission line two dielectrics, air and substrate, are not separated by a metal strip completely, so the electrical field is not contained entirely in the substrate. The mixed boundary of air and the substrate is the source of the dispersion. The accurate description of this dispersive character is important when the microstrip is used to guide pulses in various applications.

There are basically two approaches to study the electrical characteristics of a microstrip transmission line, one is to find a full solution of Maxwell equations, the other is to use a transverse electromagnetic wave (TEM) approximation.

Full wave solutions of Maxwell equations can provide the dispersive properties of microstrip as a function of frequencies. There exist several ways to find full wave solutions, such as numerical method[16], combined conformal mapping and variational method [32] and others. The most popular one among these is spectrum domain approach. Itoh and Mittra introduced the approach in 1973 [22] [23]. The idea of this method is very close to the paper by Denlinger [8] but is implemented in the spectral domain. In this approach a hybrid-mode solution is found by assuming two unknown surface current distributions on the strip. Two coupled algebraic equations are formulated by satisfying the boundary conditions in the spectral domain. These two algebraic equations are then solved by Galerkin's method, that is, via expanding the unknown current distributions in terms of known bases, a system of equations is found for unknown coefficients. By setting the determinant of the corresponding matrix equal to zero, the root is the propagation constant for each frequency. The advantage of solving the problem in the spectral domain is that the solution can be improved by increasing the number of the basis functions which are chosen to expand the surface

currents, however, the more functions used, the larger the size of the matrix. Since the speed of this method is highly dependent on the number of basis functions, the modification of this method, in order to accelerate the computation, becomes an important topic in many papers afterwards [17] [18] [35] [27] [3] [34]. Potential theory is another approach to find a full wave solution of microstrip transmission line[21] [13] [19] [7]. In this approach the electromagnetic field is expressed in terms of a vector potential and a scalar potential. Instead of finding the field solution directly, the solution for the two potentials is sought. Propagation constants are then determined by the conservation of charges and currents on the strip.

The methods related to the TEM approximation provide propagation constants at low frequencies. At low frequencies, when the wavelength is much bigger than either the height of the substrate or the width of the strip, physical reasoning is employed to justify a TEM approximation to the problem. Therefore, different approaches are given to solve the corresponding potential equations such as conformal mapping [15], variational methods [37] [36], numerical approachs [33] [26] and some others [24] [6] [10].

In this paper, a new clear systematic mathematical approach is employed directly on the Maxwell equations to solve the microstrip problem. This approach belongs to the TEM approximation category. Specifically, we employ an asymptotic method to determine an approximation to the field components and propagation constant when the wavelength is much bigger than the thickness of the substrate. It is found that the transverse electrical and magnetic fields can be expressed in terms of two potential functions which are elliptic in character and are coupled through boundary conditions of the longitudinal electrical field. The solvability conditions for the longitudinal magnetic field yield an approximation to the propagation constant. Therefore, although the longitudinal fields are much smaller than the corresponding transverse fields, they are very important and cannot be neglected. None the less, the

results we obtain do agree with the TEM approximation. Higher order corrections to the propagation constant are also given through our perturbation analysis. Then the global behavior of the propagation constant for any wavelength is obtained by the Padé approximation.

This mathematical approach can be generalized to deal with different configurations of microstrip transmission lines. For example, a transmission line equation is derived for the strip line with a smoothly changing width at low frequencies. The potential on the strip can be solved numerically for each width which is a function of z. For coupled microstrip transmission lines, coupled differential equations which describe the currents and voltages on the strips are deduced; these give rise to the equivalent circuit for these transmission lines. Each coefficient in these equations is well defined through potential functions. This approach can be used to deal with n coupled microstrip transmission lines.

Since the potential problems are solved numerically by using an integral formulation involving Green's functions, solutions can also be applied to half-shielded or shielded microstrips by changing the corresponding Green's functions. Therefore the method is valid for a large variety of configurations.

Chapters 4, 5 and 6 illustrate the problem. Chapter 4 is organized in the following way. Section 4.2 describes the mathematical formulation and assumptions of the problem. A small parameter δ is found through the nondimensionalization of the six scalar Maxwell equations. In Section 4.3, a regular perturbation analysis is implemented to the six scalar equations, that is, we expand the fields and the propagation constant in terms of δ and substitute them into the governing equations. Each order of equations is solved by introducing potential functions, then the propagation constant of each order is deduced through solvability conditions of the problem. Section 4.4 contains the Padé approximation which provides an approximation of the propagation constant for all frequencies.

4.2 Mathematical Formulation

The cross-section of the microstrip transmission line, which we consider, is sketched in Figure 4.2. It is an open microstrip. The structure is infinite in the x' and z' directions. Both the ground plane and the strip are assumed to be perfect conductors. The substrate is a lossless isotropic dielectric with permittivity and permeability being ϵ_1 and μ_0, respectively. The width of the strip w and the height of the substrate h have the same length scale, while the thickness of the strip is neglected in the analysis. For convenience we call the area above the dielectric as Region I and the area below it as Region II.

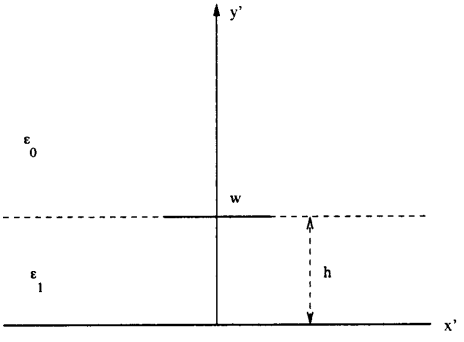

Figure 4.2 The cross-section of a microstrip transmission line.

The electromagnetic fields which describe the microstrip transmission line satisfy Maxwell's equations,

$$\nabla' \times \vec{E}' = -\mu_0 \frac{\partial \vec{H}'}{\partial t'} \tag{4.1a}$$

$$\nabla' \times \vec{H}' = \epsilon \frac{\partial \vec{E}'}{\partial t'}, \tag{4.1b}$$

where ϵ is a step function in y', taking values ϵ_1 in the substrate, and ϵ_0 in the air. On the perfect conductors the tangential components of the electric field are zero and across the air-substrate interface the tangential components of the electric and magnetic fields are continuous. The primes($'$) denote dimensional quantities.

We shall investigate the solution of the equations in the limit as h/λ_0 approaches 0, when a potential is applied between the strip and the ground plane. Here λ_0 is the wavelength equal to $2\pi c_0/\omega$ with ω being the angular frequency and c_0 being the velocity of light in vacuum. The solutions we are looking for have the form $\vec{E}'(x', y')e^{i\gamma' z' - i\omega t'}$ and $\vec{H}'(x', y')e^{i\gamma' z' - i\omega t'}$, that is, an electromagnetic wave propagating in the z' direction with a propagation constant γ'.

The two vector equations (4.1) can be written in their components forms as six scalar equations. We choose h to be the length scale of x' and y' and $\lambda_0/2\pi$ to be the length scale of z'. The dimension of E' and H' are included in E_0 and H_0 and they satisfy $H_0/E_0 = \sqrt{\epsilon_0/\mu_0}$. To keep the exponential term $-i\gamma' z'$ dimensionless, the propagation constant is scaled by $2\pi/\lambda_0$. Thus, the six nondimensional scalar equations are

$$E_{3y} - i\gamma\delta E_2 = i\delta H_1, \tag{4.2a}$$

$$-E_{3x} + i\gamma\delta E_1 = i\delta H_2, \tag{4.2b}$$

$$E_{2x} - E_{1y} = i\delta H_3, \tag{4.2c}$$

$$H_{3y} - i\gamma\delta H_2 = -iN^2\delta E_1, \tag{4.2d}$$

$$-H_{3x} + i\gamma\delta H_1 = -iN^2\delta E_2, \tag{4.2e}$$

$$H_{2x} - H_{1y} = iN^2\delta E_3. \tag{4.2f}$$

In these six equations, E_j and H_j denote the x, y, z components of electromagnetic fields, for $j = 1, 2, 3$, respectively. All the derivatives with respect to z are taken explicitly by multiplying $i\gamma$ to the corresponding field components. The index of reflection N^2 is defined as ϵ/ϵ_0, so that $N^2 = N_1^2 = \epsilon_1/\epsilon_0$ in the substrate and $N^2 = 1$ in the air. The parameter δ is defined as $\delta = 2\pi h/\lambda_0$, which is a small parameter under the low frequency assumption. The width of the strip $a = w/h$ is an order one parameter and the height of the substrate is 1.

4.3 Asymptotic Analysis

We shall solve equation (4.2) in an asymptotic manner. The small parameter δ enables us to do the regular asymptotic expansions for E_j, H_j $(j = 1, 2, 3)$ and γ, that is,

$$E_j = E_j^{(0)} + \delta E_j^{(1)} + \delta^2 E_j^{(2)} + \cdots, \qquad j = 1, 2, 3 \tag{4.3a}$$

$$H_j = H_j^{(0)} + \delta H_j^{(1)} + \delta^2 H_j^{(2)} + \cdots, \qquad j = 1, 2, 3 \tag{4.3b}$$

$$\gamma = \gamma^{(0)} + \delta\gamma^{(1)} + \delta^2\gamma^{(2)} + \cdots \tag{4.3c}$$

in which the superscript denotes the order of a function. Substituting these expansions in equation (4.2) and collecting terms with like orders of δ yield groups of differential equations involving different order of electromagnetic fields and γ. These groups of equations will be addressed one by one in the following subsections until we obtain an asymptotic expansion of γ in the limiting case as δ approaches 0.

4.3.1 Zeroth Order Equations

The coefficients of δ^0 yield the zeroth order equations,

$$E_{3x}^{(0)} = E_{3y}^{(0)} = 0, \tag{4.4a}$$

$$H_{3x}^{(0)} = H_{3y}^{(0)} = 0. \tag{4.4b}$$

Therefore both $E_3^{(0)}$ and $H_3^{(0)}$ are constants in the xy-plane. The boundary conditions that E_3 is zero on the ground plane and on the strip yield $E_3^{(0)} = 0$. The constant $H_3^{(0)}$ can be found by using the other equation involving $H_3^{(0)}$, that is : $E_{2x}^{(1)} - E_{1y}^{(1)} = iH_3^{(0)}$. Integrating this equation over the truncated version of Region I $(-L \le x \le L,$ $1 < y \le L)$ and Region II $(-L \le x \le L,\ 0 \le y < 1)$ separately and applying the divergence theorem, we have,

$$\int_{-L}^{L} E_1^{(1)}|_{y=1+} dx = iH_3^{(0)} A_I + o(1), \tag{4.5a}$$

$$-\int_{-L}^{L} E_1^{(1)}|_{y=1-} dx = iH_3^{(0)} A_{II} + o(1), \tag{4.5b}$$

where the $o(1)$ term approaches zero as L approaches ∞, provided $E_1^{(1)}$ and $E_2^{(1)}$ also approach zero as L approaches ∞. The truncated areas, Region I and Region II have areas $A_I = 2L(L-1)$ and $A_{II} = 2L$, respectively. Adding two equations (4.5) together gives

$$\begin{aligned}\int_{-L}^{L}(E_1^{(1)}|_{y=1^+} - E_1^{(1)}|_{y=1^-})dx &= iH_3^{(0)}(A_I + A_{II}) + o(1) \\ &= i2L^2H_3^{(0)} + o(1).\end{aligned} \tag{4.6}$$

From the boundary condition, E_1 is continuous across the air-dielectric interface and zero on the strip, so the left hand side of equation (4.6) is 0, which implies that $H_3^{(0)} = o(1)i/2L^2$. If L approaches ∞, then $H_3^{(0)}$ approaches 0. Hence, we deduce that $H_3^{(0)} \equiv 0$.

4.3.2 First Order Equations

The first order equations consist of six subequations. They are stated below.

$$E_{3y}^{(1)} - i\gamma^{(0)}E_2^{(0)} = iH_1^{(0)}, \tag{4.7a}$$

$$-E_{3x}^{(1)} + i\gamma^{(0)}E_1^{(0)} = iH_2^{(0)}, \tag{4.7b}$$

$$E_{2x}^{(0)} - E_{1y}^{(0)} = 0, \tag{4.7c}$$

$$H_{3y}^{(1)} - i\gamma^{(0)}H_2^{(0)} = -iN^2E_1^{(0)}, \tag{4.7d}$$

$$-H_{3x}^{(1)} + i\gamma^{(0)}H_1^{(0)} = -iN^2E_2^{(0)}, \tag{4.7e}$$

$$H_{2x}^{(0)} - H_{1y}^{(0)} = 0. \tag{4.7f}$$

Differentiating equation (4.7d) with respect to x and equation (4.7e) with respect to y, adding the two equations thus obtained, and applying equation (4.7f), we obtain $(N^2E_1^{(0)})_x + (N^2E_2^{(0)})_y = 0$. Combining this with equation (6.2c) yields two equations

for $E_1^{(0)}$ and $E_2^{(0)}$,

$$(N^2 E_1^{(0)})_x + (N^2 E_2^{(0)})_y = 0 \tag{4.8a}$$

$$E_{2x}^{(0)} - E_{1y}^{(0)} = 0. \tag{4.8b}$$

We now introduce a potential function $\Phi(x, y)$, such that $E_1^{(0)} = -\Phi_x$ and $E_2^{(0)} = -\Phi_y$. Substituting these potential representations in equation (4.8a) gives,

$$\nabla \cdot (N^2 \nabla \Phi) = 0. \tag{4.9}$$

We note that, the potential representation also satisfies equation (4.8b). On the perfect conductors Φ is a constant because $E_1^{(0)} = 0$. Without loss of generality, we choose $\Phi = 1$ on the strip and 0 on the ground plane. Across the air-dielectric interface both Φ and $N^2\Phi_y$ are continuous.

Applying the same procedure, we find two equations for $H_1^{(0)}$ and $H_2^{(0)}$,

$$H_{1x}^{(0)} + H_{2y}^{(0)} = 0, \tag{4.10a}$$

$$H_{2x}^{(0)} - H_{1y}^{(0)} = 0. \tag{4.10b}$$

A new potential function $\hat{\Psi}(x, y)$ is introduced such that $H_1^{(0)} = \hat{\Psi}_y$ and $H_2^{(0)} = -\hat{\Psi}_x$. Substituting $H_1^{(0)}$ and $H_2^{(0)}$ in equation (4.10b) implies that $\hat{\Psi}$ satisfies Laplace equation, $\nabla^2 \hat{\Psi} = 0$. The boundary conditions of $\hat{\Psi}$ can be derived in the following manner from equation (4.7). Rewriting equations (4.7a) and (4.7b) in terms of Φ and $\hat{\Psi}$ and integrating them with respect to x and y, respectively gives, $E_3^1 = i(\hat{\Psi} - \gamma^{(0)}\Phi)$. Since $E_3^{(1)} = 0$ on the perfect conductors, substituting the values of Φ implies that $\hat{\Psi} = 0$ on the ground plane and $\hat{\Psi} = \gamma^{(0)}$ on the strip. The continuity of $\hat{\Psi}$ across the air-dielectric interface is implied by the continuity of $E_3^{(1)}$ and Φ. Also, $H_1^{(0)}$ is continuous implies that $\hat{\Psi}_y$ is continuous across the air-dielectric interface.

We let $\hat{\Psi} = \gamma^{(0)}\Psi$. Hence, $H_1^{(0)} = \gamma^{(0)}\Psi_y$ and $H_2^{(0)} = -\gamma^{(0)}\Psi_x$. As mensioned

before, Ψ satisfies the Laplace equation

$$\nabla^2\Psi = 0 \tag{4.11}$$

and $\Psi = 1$ on the strip, $\Psi = 0$ on the ground plane, Ψ and Ψ_y are continuous across the air-dielectric interface.

By comparing the equations and the boundary conditions governing Φ and Ψ, we observe that the potential problem for Ψ is a special case of the potential problem for Φ in which N^2 equals 1 for both the regions.

Substituting Φ_y and Ψ_y into equation (4.7e) yields $H_{3x}^{(1)} = i((\gamma^{(0)})^2\Psi_y - N^2\Phi_y)$. We then integrate this equation with respect to x form $-\infty$ to $+\infty$ at $y = 1^+$ and $y = 1^-$, respectively, which gives

$$H_3^{(1)}(\infty, 1^+) - H_3^{(1)}(-\infty, 1^+) = i\int_{-\infty}^{\infty}((\gamma^{(0)})^2\Psi_y - N^2\Phi_y)|_{y=1^+}dx \tag{4.12a}$$

$$H_3^{(1)}(\infty, 1^-) - H_3^{(1)}(-\infty, 1^-) = i\int_{-\infty}^{\infty}((\gamma^{(0)})^2\Psi_y - N^2\Phi_y)|_{y=1^-}dx. \tag{4.12b}$$

Subtracting equation (4.12a) from equation (4.12b) and using the continuity conditions of H_3 and the potential functions with their derivatives across the air-dielectric interface, we obtain

$$\int_s((\gamma^{(0)})^2[\Psi_y] - [N^2\Phi_y])dx = 0, \tag{4.13}$$

where $\int_s$ denotes the integration over the strip and square bracket [ ] denotes the jump of a function across the strip. This is in essence a solvability or a compatibility condition for the problem. Solving for $\gamma^{(0)}$ gives

$$(\gamma^{(0)})^2 = \frac{\int_s[N^2\Phi_y]dx}{\int_s[\Psi_y]dx}. \tag{4.14}$$

This is the leading order nondimensionalized propagation constant.

The square of the leading order propagation constant $(\gamma^{(0)})^2$ can take any value between 1 and N_1^2. This fact can be obtained mathematically using the potential

representation in equation (4.14) and Cauchy-Schwarz inequality. The proof is in Appendix E.

There are several ways to compute the potential functions Φ and Ψ numerically, so that $\gamma^{(0)}$ can be found using equation (4.14). In Chapter 6, we will construct integral equations to each of the potentials. Solving the integral equations numerically gives the functions $[N^2\Phi_y]$ and $[\Psi_y]$ on the strip directly, and thereby, giving a numerical approximation for $(\gamma^{(0)})^2$.

We now conclude the findings of this subsection. The zeroth order transverse electromagnetic fields are

$$E_1^{(0)} = -\Phi_x, \qquad E_2^{(0)} = -\Phi_y, \tag{4.15a}$$

$$H_1^{(0)} = \gamma^{(0)}\Psi_y, \qquad H_2^{(0)} = -\gamma^{(0)}\Psi_x. \tag{4.15b}$$

The first order longitudinal electrical field is

$$E_3^{(1)} = i(\gamma^{(0)}\Psi - \gamma^{(0)}\Phi), \tag{4.16}$$

and the first order longitudinal magnetic field is written in terms of its derivatives,

$$H_{3x}^{(1)} = i(\gamma^{(0)})^2\Psi_y - iN^2\Phi_y, \tag{4.17a}$$

$$H_{3y}^{(1)} = -i(\gamma^{(0)})^2\Psi_x + iN^2\Phi_x. \tag{4.17b}$$

We observe that, the zeroth order transverse fields are nonzero, while the zeroth order longitudinal fields are zero from Section 4.3.1. Therefore, the transverse fields are order one quantities while the longitudinal fields have order δ. This is consistent with the result that, at low frequencies, a microstrip transmission line has a quasi-TEM wave. That is, at low frenquencies, although the longitudinal fields are nonzero in the microstrip, their magnitudes are relatively small compared to the magnitudes of the transverse fields. We have proved this result mathematically using the asymptotic analysis.

We also notice that, although the longitudinal fields are much smaller than the corresponding transverse fields, they are very important and cannot be neglected. Since the two potential functions Φ and Ψ are coupled through the boundary conditions of the longitudinal electrical field, and the solvability condition for the longitudinal magnetic field yields the propagation constant.

4.3.3 Second Order Equations

We now consider the second order system

$$E_{3y}^{(2)} - i\gamma^{(0)}E_2^{(1)} - i\gamma^{(1)}E_2^{(0)} = iH_1^{(1)}, \tag{4.18a}$$

$$-E_{3x}^{(2)} + i\gamma^{(0)}E_1^{(1)} + i\gamma^{(1)}E_1^{(0)} = iH_2^{(1)}, \tag{4.18b}$$

$$E_{2x}^{(1)} - E_{1y}^{(1)} = 0, \tag{4.18c}$$

$$H_{3y}^{(2)} - i\gamma^{(0)}H_2^{(1)} - i\gamma^{(1)}H_2^{(0)} = -iN^2E_1^{(1)}, \tag{4.18d}$$

$$-H_{3x}^{(2)} + i\gamma^{(0)}H_1^{(1)} + i\gamma^{(1)}H_1^{(0)} = -iN^2E_2^{(1)}, \tag{4.18e}$$

$$H_{2x}^{(1)} - H_{1y}^{(1)} = 0. \tag{4.18f}$$

Analyzing equations (4.18) just as we analyzed the first order system (equations (4.7)) implies that $E_1^{(1)}$ and $E_2^{(1)}$ satisfy the same equations as were satisfied by $E_1^{(0)}$ and $E_2^{(0)}$. However, the potential applied across the strip and the ground plane does not depend upon δ. Therefore, we conclude that $E_1^{(1)} = E_2^{(1)} = 0$. By using the same technique employed to find $H_1^{(0)}$ and $H_2^{(0)}$, we deduce that $H_1^{(1)} = \gamma^{(1)}\Psi_y$ and $H_2^{(1)} = -\gamma^{(1)}\Psi_x$. Substituting for $H_1^{(1)}$, $H_1^{(0)}$ and $E_2^{(1)}$ in equation (4.18e) and carrying out the same analysis for $H_{3x}^{(2)}$, as was done for $H_{3x}^{(1)}$, we obtain that $2\gamma^{(0)}\gamma^{(1)}\int_s[\Psi_y]dx = 0$. Therefore,

$$\gamma^{(1)} = 0. \tag{4.19}$$

Consequently, $H_1^{(1)} = H_2^{(1)} = 0$, and both $E_3^{(2)}$ and $H_3^{(2)}$ are constants. Just as we determined that $E_3^{(0)}$ and $H_3^{(0)}$ are zero, we now conclude that both $E_3^{(2)}$ and $H_3^{(2)}$ are

also zeroes.

The system of second order equations does not give a nonzero higher order correction term for γ. Hence, we seek the correction term in the system of equations of the third order.

4.3.4 Third Order Equations

We now consider the third order system. This system also comprises six equations, stated as,

$$E_{3y}^{(3)} - i\gamma^{(0)}E_2^{(2)} - i\gamma^{(2)}E_2^{(0)} = iH_1^{(2)}, \tag{4.20a}$$

$$-E_{3x}^{(3)} + i\gamma^{(0)}E_1^{(2)} + i\gamma^{(2)}E_1^{(0)} = iH_2^{(2)}, \tag{4.20b}$$

$$E_{2x}^{(2)} - E_{1y}^{(2)} = iH_3^{(1)}, \tag{4.20c}$$

$$H_{3y}^{(3)} - i\gamma^{(0)}H_2^{(2)} - i\gamma^{(2)}H_2^{(0)} = -iN^2E_1^{(2)}, \tag{4.20d}$$

$$-H_{3x}^{(3)} + i\gamma^{(0)}H_1^{(2)} + i\gamma^{(2)}H_1^{(0)} = -iN^2E_2^{(2)}, \tag{4.20e}$$

$$H_{2x}^{(2)} - H_{1y}^{(2)} = -iN^2E_3^{(1)}. \tag{4.20f}$$

By applying the same method as was applied to the first and second order systems, we obtain two equations in two unknowns $E_1^{(2)}$ and $E_2^{(2)}$,

$$(N^2E_1^{(2)})_x + (N^2E_2^{(2)})_y = -i\gamma^{(0)}N^2E_3^{(1)}, \tag{4.21a}$$

$$E_{2x}^{(2)} - E_{1y}^{(2)} = iH_3^{(1)}. \tag{4.21b}$$

Unlike equations (4.8), the two differential equations (4.21) have non-zero terms on the right hand sides, which are the first order longitudinal electromagnetic fields.

We will solve for the two functions $E_1^{(2)}$ and $E_2^{(2)}$ again by introducing an unknown potential function $\hat{\Gamma}$. However, because the right hand sides of equations (4.21) are non-zero, we will add an auxiliary function Ω to the transverse electric

fields. Hence, we let

$$E_1^{(2)} = -\hat{\Gamma}_x, \tag{4.22a}$$

$$E_2^{(2)} = -\hat{\Gamma}_y + \Omega. \tag{4.22b}$$

Substituting equations (4.22) in equation (4.21b) yields $\Omega_x = iH_3^{(1)}$. Differentiating Ω_x with respect to y and applying the results for $H_{3y}^{(1)}$ from equation (4.17b) imply that

$$\Omega xy = iH_{3y}^{(1)} = (\gamma^{(0)})^2\Psi_x - N^2\Phi_x. \tag{4.23}$$

Equation (4.23) allows us to choose $\Omega_y = (\gamma^{(0)})^2\Psi - N^2\Phi$. Thus, we have found both the x and y derivatives of the auxiliary function Ω. We observe that, function Ω is continuous across the air-dielectric interface, but function Ω_y is discontinuous across the air-dielectric interface.

Substituting from equations (4.22) in equation (4.21a) gives the differential equation

$$\nabla \cdot (N^2\nabla\hat{\Gamma}) = N^2((\gamma^{(0)})^2 - N^2)\Phi + (1 - N_1^2)\Omega\delta(y-1) \tag{4.24}$$

satisfied by $\hat{\Gamma}$. The second term on the right hand side of equation (4.24) has a factor $\delta(y-1)$ which denotes the Kronecker delta. The presence of the Kronecker delta factor is attributed to the y derivative of the step function N^2. The boundary conditions of $\hat{\Gamma}$ are obtained from equations (4.22). Since $E_1^{(2)} = 0$ on the strip and on the ground plane, $\hat{\Gamma}$ is a constant. We set $\hat{\Gamma} = 0$ on the ground plane, and $\hat{\Gamma} = \alpha$ on the strip, where α is an unknown real number. Later we will show that the value of α will not affect the result of the second order propagation constant $\gamma^{(2)}$. Function $\hat{\Gamma}$ is continuous across the air-dielectric interface. The behavior of the normal derivative of $\hat{\Gamma}$ across the air-dielectric interface is governed by the equation (4.24).

Equation (4.24) prescribing $\hat{\Gamma}$ is nonhomogeneous and so is its boundary condition

on the strip ($\hat{\Gamma} = \alpha$). Hence, we let $\hat{\Gamma} = \alpha\Phi + \Gamma$. The first term $\alpha\Phi$ takes into account the nonhomogeneous boundary condition, the second term Γ also satisfies equation (4.24) but is subject to homogeneous boundary conditions. Therefore, the two field components can now be written as

$$E_1^{(2)} = -\alpha\Phi_x - \Gamma_x, \tag{4.25a}$$

$$E_2^{(2)} = -\alpha\Phi_y - \Gamma_y + \Omega, \tag{4.25b}$$

where Γ satisfies the equation

$$\nabla \cdot (N^2 \nabla\Gamma) = N^2((\gamma^{(0)})^2 - N^2)\Phi + (1 - N_1^2)\Omega\delta(y-1). \tag{4.26}$$

Function Γ is zero on both the strip and the ground plane, and continuous across the air-dielectric interface.

The transverse magnetic fields $H_1^{(2)}$ and $H_2^{(2)}$ satisfy the following two equations.

$$H_{1x}^{(2)} + H_{2y}^{(2)} = -i\gamma^{(0)} H_3^{(1)}, \tag{4.27a}$$

$$H_{2x}^{(2)} - H_{1y}^{(2)} = -iN^2 E_3^{(1)}. \tag{4.27b}$$

The right hand of the equations are non-zero as well. We let $H_1^{(2)} = \hat{P}_y - \gamma^{(0)}\Omega$, and $H_2^{(2)} = -\hat{P}_x$, where $\hat{P}$ is an unknown function. Then, equation (4.27a) is satisfied. We substitute for $H_1^{(2)}$ and $H_2^{(2)}$ in equation (4.27b) and obtain a Poisson equation for $\hat{P}$ with the source term being $\gamma^{(0)}((\gamma^{(0)})^2 - N^2)\Psi$. The unknown $\hat{P}$ is constant on both the ground plane and the strip because $H_2^{(2)}$ vanishes at these planes. However, the constants are not arbitrary. Substituting the potential representations of $H_1^{(2)}$, $H_2^{(2)}$, $E_1^{(2)}$, $E_2^{(2)}$ in equations (4.20a) and (4.20b), we find that $E_3^{(3)} = -i\{(\alpha\gamma^{(0)} + \gamma^{(2)})\Phi + \gamma^{(0)}\Gamma - \hat{P}\}$. Since $E_3^{(3)} = 0$ on both of the metal surfaces, function $\hat{P}$ takes the value 0 on the ground plane and $\gamma^{(0)}\alpha + \gamma^{(2)}$ on the strip. Across the air-dielectric interface, $\hat{P}$ is continuous because $H_2^{(2)}$ is continuous. The normal derivative $\hat{P}_y$ is

also continuous across the interface since both $H_1^{(2)}$ and Ω are continuous.

Both the equation and the boundary conditions of $\hat{P}$ are nonhomogeneous. Now, we set $\hat{P} = (\gamma^{(0)}\alpha + \gamma^{(2)})\Psi + \gamma^{(0)}P$, following the same procedure that was applied to $\hat{\Gamma}$. Thus, the two nonhomogeneous terms in $\hat{P}$ are separated. Therefore, $H_1^{(2)}$ and $H_2^{(2)}$ can be written as

$$H_1^{(2)} = (\gamma^{(0)}\alpha + \gamma^{(2)})\Psi_y + \gamma^{(0)}P_y - \gamma^{(0)}\Omega \tag{4.28a}$$

$$H_2^{(2)} = -(\gamma^{(0)}\alpha + \gamma^{(2)})\Psi_x - \gamma^{(0)}P_x, \tag{4.28b}$$

where P satisfies

$$\nabla^2 P = ((\gamma^{(0)})^2 - N^2)\Psi, \tag{4.29}$$

and $P = 0$ on both the ground plane and the strip.

Applying the same argument, as was used in deriving $\gamma^{(0)}$, an expression for $\gamma^{(2)}$ from equation (4.20e) is obtained.

$$\gamma^{(2)} = -\frac{\int_s [N^2 E_2^{(2)}]dx + \gamma^{(0)} \int_s [H_1^{(2)}]dx}{\gamma^{(0)} \int_s [\Psi_y]dx}. \tag{4.30}$$

Substituting the potential representations of $H_1^{(2)}$ and $E_2^{(2)}$ from equations (4.25b) and (4.28a), respectively, in equation (4.30) gives,

$$\gamma^{(2)} = \frac{\int_s [N^2\Gamma_y - N^2\Omega]dx - (\gamma^{(0)})^2 \int_s [P_y - \Omega]dx}{2\gamma^{(0)} \int_s [\Psi_y]dx}. \tag{4.31}$$

In the representation for $\gamma^{(2)}$ in equation (4.31), the unknown parameter α doesn't appear, since the coefficient of α is $\int_s \{[N^2\Phi_y] - (\gamma^{(0)})^2[\Psi_y]\}dx$ which equals 0. Hence, the value of the potential $\hat{\Gamma}$ on the strip doesn't contribute to the expression for $\gamma^{(2)}$.

4.4 Propagation Constant γ

4.4.1 An Approximation of γ at Low Frequencies

The asymptotic analysis in Section 4.3 can be carried out for the fourth order system and gives $\gamma^{(3)} = 0$. Hence, when δ is very small, the propagation constant is approximated by

$$\gamma = \gamma^{(0)} + \delta^2\gamma^{(2)} + O(\delta^4). \tag{4.32}$$

After we recover the dimension, the dimensional propagation constant $\gamma' = (\gamma^{(0)} + (\frac{\omega h}{c_0})^2\gamma^{(2)} + \cdots)\frac{\omega}{c_0}$. The phase velocity v_p and the group velocity v_g of the transmission line can now be written approximately as

$$v_p = \frac{\omega}{\gamma'} = \frac{c_0}{\gamma^{(0)} + (\frac{\omega h}{c_0})^2\gamma^{(2)} + \cdots}, \tag{4.33a}$$

$$v_g = \frac{d\omega}{d\gamma'} = \frac{c_0}{\gamma^{(0)} + 3(\frac{\omega h}{c_0})^2\gamma^{(2)} + \cdots}. \tag{4.33b}$$

Hence, at low frequencies, the second order and higher order corrections to γ' describe the dispersion properties of a microstrip transmission line quantitatively.

Another parameter ϵ_{eff}, the effective dielectric constant, is often used to describe the dispersion of microstrip transmission lines instead of the propagation constant γ. These two parameters are related by $\gamma^2 = \epsilon_{eff}$. Therefore, at low frequencies the effective dielectric constant can be approximated as,

$$\begin{aligned} \epsilon_{eff} = \gamma^2 &= (\gamma^{(0)})^2 + 2\gamma^{(0)}\gamma^{(2)}\delta^2 + O(\delta^4) \\ &= (\gamma^{(0)})^2 + (2\gamma^{(0)}\gamma^{(2)}) \cdot \left(\frac{2\pi h}{c_0}\right)^2 \cdot f^2 + \cdots . \end{aligned} \tag{4.34}$$

where f is the frequency.

4.4.2 The Limit of γ at High Frequencies

Until now, we considered the case when the wavelength λ_0 is much greater than the height h of the substrate. In this section, we will find γ in the other limit, that is,

when the wavelength λ_0 is much smaller than the height h of the substrate (h/λ_0 approaches ∞).

We nondimensionalize the problem as before. The equations obtained are exactly as equations (4.2). Since $\delta = 2\pi h/\lambda_0$, now we consider the case when δ is much greater than 1. We divide these six equations by δ and do the regular asymptotic expansions to the field components and the propagation constant. The first order equations are

$$\gamma_\infty E_2 = -H_1, \qquad \gamma_\infty H_2 = N^2 E_1, \tag{4.35a}$$

$$\gamma_\infty E_1 = H_2, \qquad \gamma_\infty H_1 = -N^2 E_2. \tag{4.35b}$$

Simple algebraic operations yield,

$$\gamma_\infty^2 = N^2. \tag{4.36}$$

In this limit, N^2 is not a step function any more. Since when λ_0 is fixed, as h approaches ∞, we have $N^2 = N_1^2$. Therefore, $\gamma_\infty^2 = N_1^2$. This result is known [29], and can be explained intuitively as follows. When λ_0 is fixed and h approaches ∞, signals propagate within the dielectric. The effective dielectric constant $\epsilon_{eff} = \gamma^2 = N_1^2$, which is just the index of reflection of the dielectric.

4.4.3 Padé Approximation

To obtain the propagation constant γ as a function of frequency, we will use the behavior of γ in the two limiting cases (low frequencies and high frequencies) and the asymptotic expansion of γ at low frequencies.

Padé approximation is carried out for γ^2 by writing γ^2 as a quotient of two polynomials

$$\gamma^2 = \frac{a + bf^2}{c + df^2} = \frac{\bar{a} + \bar{b}f^2}{1 + \bar{d}f^2}. \tag{4.37}$$

We choose γ^2 to be an even function of f because the low frequency expansion of γ^2 is an even function. There are three parameters $\bar{a}$, $\bar{b}$ and $\bar{d}$ which need to be determined. It is known that

$$\gamma^2 \to \begin{cases} (\gamma^{(0)})^2 & f \to 0 \\ N_1^2 & f \to \infty, \end{cases} \tag{4.38}$$

which implies that $\bar{a} = (\gamma^{(0)})^2$ and $\bar{b}/\bar{d} = N_1^2$. The Taylor expansion of equation (4.37) for small value of f compared to equation (4.34) gives,

$$\bar{d} = \frac{2\gamma^{(0)}\gamma^{(2)}(\frac{2\pi h}{c_0})^2}{N_1^2 - (\gamma^{(0)})^2}. \tag{4.39}$$

Therefore, γ^2 is approximated as

$$\gamma^2 = N_1^2 - \frac{N_1^2 - (\gamma^{(0)})^2}{1 + \bar{d}f^2}, \tag{4.40}$$

where $\bar{d}$ is defined in equation (4.39). In Chapter 5, we will compute γ^2 numerically.

CHAPTER 5

NUMERICAL RESULTS OF PROPAGATION CONSTANT

In Chapter 4, we used asymptotic analysis to deduce expressions for $\gamma^{(0)}$ and $\gamma^{(2)}$. These expressions are determined by four integrals on the strip (equations (4.14) and (4.31)). Each of these integrals is related to a potential function. In this chapter, we will compute these integrals numerically.

One way to solve Laplace equations or Poisson equations for each potential is by using the finite difference method. The jumps of the normal derivatives of these potential functions across the strip can then be obtained approximately using finite difference approximation. After that, the integrals of these jumps over the strip can be computed by Trapezoidal Rule or Simpson's Rule . This method is easy to implement but time consuming, if a reasonably accurate result is desired. Therefore, we choose to employ Green's functions to find integral equations of the unknown potentials and then solve the integral equations numerically. In this way, we can directly obtain the jumps of the normal derivative of the potential functions across the strip.

This chapter contains two sections. The first section contains the numerical solution of $\gamma^{(0)}$ and the second section contains the results of γ for all frequencies.

5.1 Numerical Results of $\gamma^{(0)}$

The square of the leading order propagation constant $(\gamma^{(0)})^2$ is the quotient of two functions, $\int_s [N^2\Phi_y]dx$ and $\int_s [\Psi_y]dx$ from equation (4.14). In Chapter 4, we saw that both Φ and Ψ satisfy Laplace equation and take the value 1 on the strip and 0 on the ground plane. Also, both Φ and Ψ are continuos across the air-dielectric interface. We also observed that function Ψ is just a special case of function Φ, when N^2 is constant and equals 1 in both regions, Region I and Region II. Therefore, if we can construct an integral representation for the unknown function Φ, then a similar

integral representation of Ψ will be obtained in a straightforward manner by setting $N^2 = 1$.

We consider a half-space Green's function G which satisfies,

$$\nabla \cdot (N^2 \nabla G) = \delta(x - x')\delta(y - y'), \tag{5.1a}$$

$$G = 0 \qquad at \qquad y = 0 \tag{5.1b}$$

$$[G] = [N^2 G_y] = 0 \qquad at \qquad y = 1 \tag{5.1c}$$

where (x', y') is the position of the point source. In the function G, $N^2 = N_1^2$ when $0 < z < 1$ and $N^2 = 1$ when $1 < z < \infty$. Multiplying equation (5.1a) by Φ and equation (4.9) by G and then subtracting one from the other gives,

$$\nabla \cdot (N^2 \Phi \nabla G - N^2 G \nabla \Phi) = \Phi \delta(x - x')\delta(y - y'). \tag{5.2}$$

Integrating equation (5.2) over Region II and assuming that (x', y') is in Region II we deduce that

$$\int_{-\infty}^{\infty} (N_1^2 \Phi G_y - N_1^2 G \Phi_y)|_{y=1^-} dx = \Phi(x', y'), \tag{5.3}$$

by applying the divergence theorem and the boundary conditions for Φ and G: at $y = 0$ both Φ and G are zero; at infinity, both Φ and G are of order $1/r$. Similarily, integrating equation (5.2) over Region I and applying the divergence theorem and boundary conditions gives,

$$\int_{-\infty}^{\infty} (-\Phi G_y + G \Phi_y)|_{y=1^+} dx = 0. \tag{5.4}$$

Adding equations (5.3) and (5.4) and using the boundary conditions across the air-dielectric interface, gives an integral representation for the function Φ.

$$\Phi(x', y') = \int_s G(x, 1|x', y')[N^2 \Phi_y] dx. \tag{5.5}$$

In equation (5.5), the point source (x', y') is Region II. If we set (x', y') in Region I, we obtain the same equation. Therefore, equation (5.5) is an integral representation of Φ for $y' > 0$ in terms of the unknown function $[N^2\Phi_y]$ across the strip.

Given the condition that $\Phi = 1$ on the strip, we set $y' = 1$. Equation (5.5) can now be written as

$$\int_s G(x, 1|x', 1)[N^2\Phi_y]dx = 1, \tag{5.6}$$

which is an integral equation for the unknown $[N^2\Phi_y]$.

When N^2 equals 1 in both regions, we obtain an integral representation of Ψ and an integral equation for $[\Psi_y]$. That is,

$$\Psi(x', y') = \int_s G(x, 1|x', y')[\Psi_y]dx, \tag{5.7}$$

and

$$\int_s G(x, 1|x', 1)[\Psi_y]dx = 1. \tag{5.8}$$

In these two equations the Green's function G also has $N^2 = 1$ for $y' > 0$.

Equations (5.6) and (5.8) will be solved numerically by Galerkin's method, and the distributions of $[N^2\Phi_y]$ and $[\Psi_y]$ over the strip will be given. The value of $(\gamma^{(0)})^2$ is found consequently by integrating these two functions over the strip numerically.

The Green's function that we use to solve for $[N^2\Phi_y]$ is found using Fourier integral transformation (the details are shown in Appendix F). It is,

$$G(x, 1|x', 1) = \frac{1}{2\pi(1 + N_1^2)} \sum_{n=0}^{\infty} (-\rho)^n \ln \frac{(2n)^2 + (x - x')^2}{(2n + 2)^2 + (x - x')^2} \tag{5.9}$$

where $\rho = (N_1^2 - 1)/(N_1^2 + 1) < 1$. When $N_1^2 = 1$, only the $n = 0$ term survives. Function G can be simplified as

$$G(x, 1|x', 1) = \frac{1}{4\pi} \ln \frac{(x - x')^2}{4 + (x - x')^2}. \tag{5.10}$$

This Green's function in (5.10) is then used in equation (5.8) to solve for the unknown $[\Psi_y]$.

The following two plots, Figures 5.1 and 5.2 are the distribution of $[N^2\Phi_y]$ and $[\Psi_y]$ on the strip, respectively. Both $[N^2\Phi_y]$ and $[\Psi_y]$ show singularities at the edges of the strip. Particularly, in Figure 5.2, the singularity of function $[\Psi_y]$ behaves like $(x - a/2)^{-1/2}$ near the edges [11]. In Figure 5.3, the results of $(\gamma^{(0)})^2$ are given when $N_1^2 = 12.9$ for different widths of the strip. Comparison of our results with other existing results [19] yields a very good agreement. From Figure 5.3 we observe that for the same substrate, the leading order propagation constant $\gamma^{(0)}$ is increasing as the width of the strip a becomes larger, and $(\gamma^{(0)})^2$ approaches N_1^2 as a approaches infinity.

We solve the potential problems by using the half space Green's function (equation

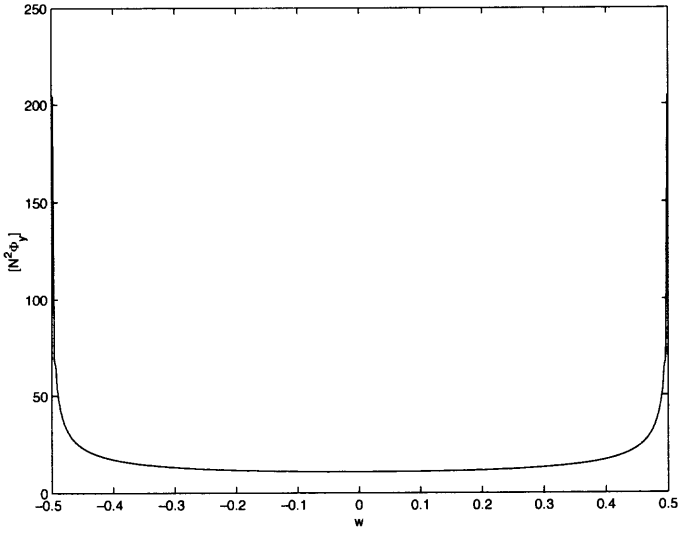

Figure 5.1 The distribution of $[N^2\Phi_y]$ on the strip when $N_1^2 = 8.0$

(5.9)) in the integral equations. This Green's function approaches 0 at infinity. More specifically, the Green's function behaves like $1/r$ at infinity. In the next step, we will construct integral equations for $[N^2\Gamma_y]$ and $[P_y]$ to compute $\gamma^{(2)}$. If we still use the same Green's function, we will run into computational problems, since the source

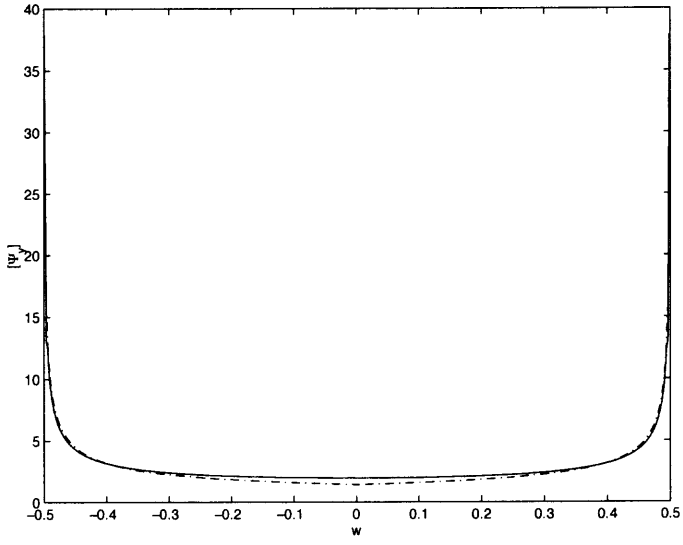

Figure 5.2 The distribution of $[\Psi_y]$ on the strip. Solid line denotes $[\Psi_y]$, dash-dot line denotes $(x - a/2)^{-1/2}$.

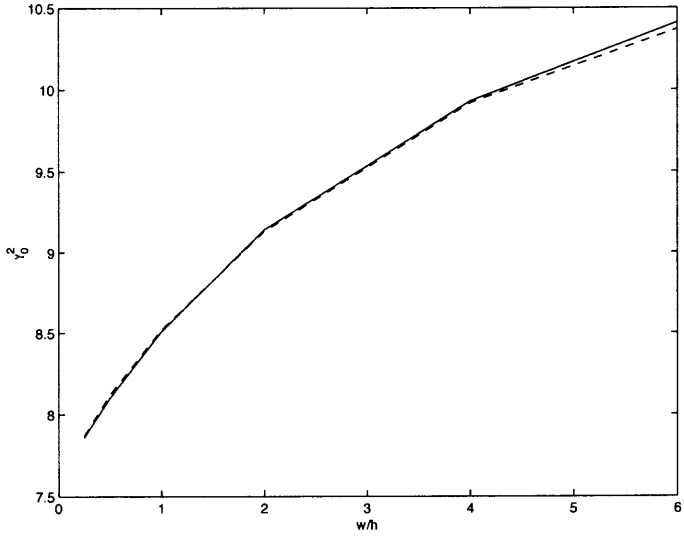

Figure 5.3 The leading order propagation constant for $N_1^2 = 12.9$ versus the width of the strip. Dashed line denotes our results, and solid line denotes the results from [19].

terms in the Poisson equations for Γ and P do not have compact supports. Therefore, we introduce a new Green's function with two boundaries at $x = \pm L/2$, where L is a large number and $G = 0$ at these two boundaries. We call this new function as half shielded Green's function and find it through separation of variables.

$$\begin{aligned} G_h(x,1|x',1) = &\sum_{m=1,3}^{\infty} \frac{-2}{m\pi} \cos\left(\frac{m\pi x}{L}\right) \cos\left(\frac{m\pi x'}{L}\right) \frac{1}{N_1^2 \coth\left(\frac{m\pi}{L}\right) + 1} \\ &+ \sum_{n=2,4}^{\infty} \frac{-2}{n\pi} \sin\left(\frac{n\pi x}{L}\right) \sin\left(\frac{n\pi x'}{L}\right) \frac{1}{N_1^2 \coth\left(\frac{n\pi}{L}\right) + 1}. \end{aligned} \tag{5.11}$$

Since both Φ and Ψ are even functions of x, the unknowns $[N^2\Phi_y]$ and $[\Psi_y]$ are also even functions of x. So in numerical computations, we will use only the cosine part of this Green's function. The contribution from the sine part is zero. By setting $N_1^2 = 1$, function G_h is used to solve integral equation (5.8)

The results of $(\gamma^{(0)})^2$ by applying half space Green's function and half shielded Green's function are compared in Figure 5.4. From Figure 5.4, we observe that the difference of the results are not distinct, and the larger the L gets, the smaller is the difference between $(\gamma^{(0)})^2$ from the two kinds of Green's functions. Therefore, we will use this half shielded Green's function instead of the half space Green's function in the next section.

5.2 Numerical Implementation of $\gamma^{(2)}$

In this section, we will obtain a numerical approximation to $\gamma^{(2)}$. From equation (4.31) we observe that the jumps of four functions $[N^2\Gamma_y]$, $[P_y]$, $[N^2\Omega]$and $[\Omega]$ across the strip need to be computed in order to compute $\gamma^{(2)}$. In the following sections we will show how to find each of them.

5.2.1 The Auxiliary Function Ω

Function Ω was introduced when we solved nonhomogeneous equations (4.21) and (4.27) for the transverse electromagnetic fields. Its x derivative and y derivative are

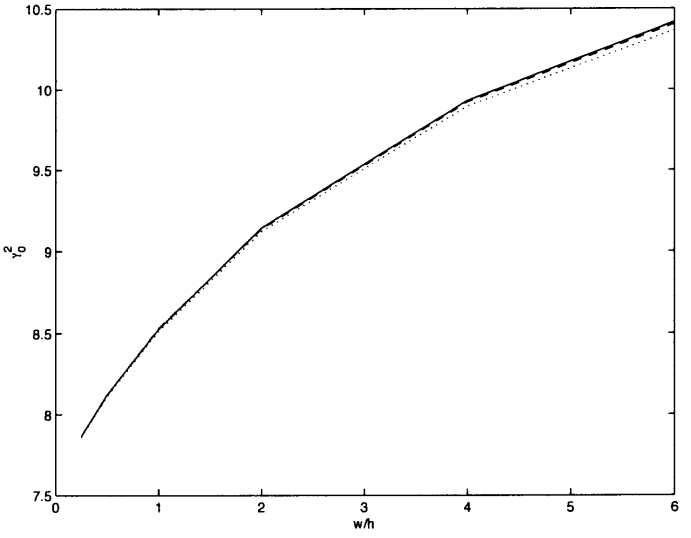

Figure 5.4 The leading order propagation constant $(\gamma^{(0)})^2$ for different Green' functions when $N_1^2 = 12.9$. Solid line denotes the result from free space Green's function; Dashed line denotes the result from half shielded Green's function for $L = 30$; Dotted line denotes the result from the half shielded Green's function for $L = 60$.

defined as

$$\Omega_x = iH_3^{(1)}, \tag{5.12a}$$

$$\Omega_y = (\gamma^{(0)})^2\Psi - N^2\Phi, \tag{5.12b}$$

respectively, from Section 4.3.4. If we take x derivative to equation (5.12a) and y derivative to equation (5.12b) and add them, we obtain a Laplace equation for Ω. This Laplace equation is not easy to solve because of the Neumann boundary conditions of Ω. However, since we only need the values of $[N^2\Omega]$ and $[\Omega]$ across the strip, we will obtain them directly. Integrating equation (5.12a) with respect to x from $-L/2$ to x at $y = 1^+$ and $y = 1^-$, respectively, gives

$$\Omega(x, 1^{\pm}) = \int_{-L/2}^{x} iH_3^{(1)}(x', 1^{\pm})dx', \tag{5.13}$$

where we assume that $\Omega = 0$ on the side walls ($x = \pm L/2$). In equation (5.13), functions $H_3^{(1)}(x', 1^{\pm})$ are obtained by integrating $H_{3x}^{(1)}$ along two lines $y = 1^{\pm}$, that is,

$$H_3^{(1)}(x, 1^{\pm}) = \int_{-L/2}^{x} H_{3x}^{(1)}(x', 1^{\pm})dx'. \tag{5.14}$$

Now, we substitute equation (5.14) in equation (5.13). After interchanging the order of integration, we find

$$\Omega(x, 1^{\pm}) = \int_{-L/2}^{x} (x - x')H_{3x'}^{(1)}|_{y=1^{\pm}}dx'. \tag{5.15}$$

Hence, if we know $H_{3x}^{(1)}$ at $y = 1^{\pm}$, we can compute Ω at $y = 1^{\pm}$. Then the jumps of $[\Omega]$ and $[N^2\Omega]$ across the strip can be obtained.

We now show how to compute $H_{3x}^{(1)}$ at $y = 1^{\pm}$ numerically. From equation (4.17a), we have $H_{3x}^{(1)} = i(\gamma^{(0)})^2\Psi_y - iN^2\Phi_y$. Therefore, we need to find Φ_y and Ψ_y at $y = 1^{\pm}$, respectively. Taking y derivative to $\Phi(x, y)$ in equation (5.5) yields:

$$\Phi_y(x, y)|_{y=1^{\pm}} = \int_s [N^2\Phi_y]\frac{\partial G_h}{\partial y}(x', 1|x, y)|_{y=1^{\pm}}dx', \tag{5.16}$$

where function $[N^2\Phi_y]$ across the strip was found in Section 5.1. The Green's function $G_h(x', 1, |x, y)$ for $y \neq 1$ in equation (5.16) are found by using separation of variables and can be written explicitly as,

$$G_h(x', 1|x, y) = \sum_{m=1,3}^{\infty} \frac{-2}{m\pi} \frac{\cos\left(\frac{m\pi x'}{L}\right)\cos\left(\frac{m\pi x}{L}\right)}{N_1^2\cosh\left(\frac{m\pi}{L}\right) + \sinh\left(\frac{m\pi}{L}\right)} \sinh\left(\frac{m\pi}{L}y\right) \quad (y < 1), \tag{5.17a}$$

$$G_h(x', 1|x, y) = \sum_{m=1,3}^{\infty} \frac{-2}{m\pi} \frac{\cos\left(\frac{m\pi x'}{L}\right)\cos\left(\frac{m\pi x}{L}\right)}{N_1^2\cosh\left(\frac{m\pi}{L}\right) + \sinh\left(\frac{m\pi}{L}\right)} \sinh\left(\frac{m\pi}{L}\right)e^{m\pi(1-y)/L} \quad (y > 1). \tag{5.17b}$$

We didn't include the sine parts of the Green's functions $G_h(x', 1|x, y)$ in (5.17) because the sine parts don't contribute anything to the integral. By knowing this $G_h(x', 1|x, y)$, the integral in equation (5.16) can be evaluated numerically and we

obtain Φ_y at $y = 1^{\pm}$. The same computation yields Ψ_y at $y = 1^{\pm}$ if we set $N_1^2 = 1$ in equation (5.16). Combining the two results of Φ_y and Ψ_y at $y = 1^{\pm}$ gives $H_{3x}^{(1)}$ at $y = 1^{\pm}$ (by using equation (4.17a)).

5.2.2 Solutions of the Two Poisson Equations

The same Green's function argument is applied to equation (4.26). Hence, the integral equation for $[N^2\Gamma_y]$ is

$$\begin{aligned}\int_s G_h(x,1|x',1)[N^2\Gamma_y]dx &= \iint_{I+II} N^2(N^2-\gamma_0^2)\Phi(x,y)G_h(x,y|x',1)dxdy \\ &\quad - \int_{off} G_h(x,1|x',1)[N^2]\Omega(x,1)dx \\ &= I_1 - I_2,\end{aligned} \tag{5.18}$$

where $\int_{off}$ denotes an integral off strip on $y = 1$.

The double integral over the half plane is obtained in the following way. We substitute the integral representation of Φ (equation (5.5)) in the double integral I_1 and interchange the order of integration, then I_1 becomes,

$$I_1 = \int_s [N^2\Phi_y](x'') \left(\iint_{I+II} N^2(N^2-\gamma_0^2)G_h(x,y|x',1)G_h(x'',1|x,y)dxdy \right) dx''. \tag{5.19}$$

Since the Green's function G_h is in terms of Fourier series, when they are multiplied and integrated with respect to x, most terms vanish. Therefore, the integral in the big parentheses in equation (5.19) are simplified as a single Fourier series. In this way the numerical computation time is dramatically reduced and the accuracy is increased. In integral I_2 the values of Ω on the line $y = 1$ is computed in Section 5.2.1.

Similarly, The integral equation for $[P_y]$ is,

$$\int_s G_h(x,1|x',1)[P_y]dx = \iint_{I+II} (N^2-\gamma_0^2)\Psi(x,y)G_h(x,y|x',1)dxdy. \tag{5.20}$$

The double integral in the right hand side of this equation is computed using the same way as was done to the previous equation (5.18).

5.3 Numerical Results

In Section 5.2, we discussed the method to obtain $\gamma^{(2)}$ numerically. By substituting both $\gamma^{(0)}$ and $\gamma^{(2)}$ in the equation (4.40), the effective dielectric constant $\epsilon_{eff} = \gamma^2$ is shown in Figure 5.5. In Figure 5.5, we choose $N_1^2 = 12.9$ when the dimensionless strip width $a = w/h$ are $0.5, 1, 2$, respectively.

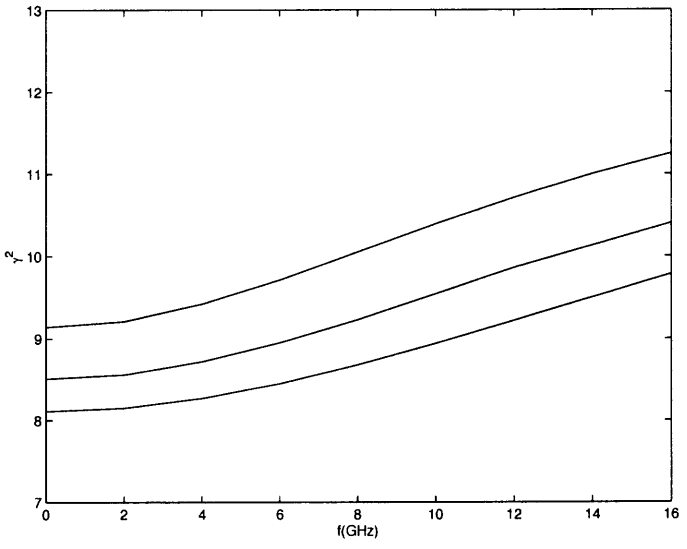

Figure 5.5 The plot of function γ^2 when $N_1^2 = 12.9$. From top to bottom, the three lines represent γ^2 when a equals 2, 1 and 0.5, resprectively.

In Figure 5.6 we compare the values of the effective dielectric constant by using different approximations for $N_1^2 = 12.9$ and $w/h = 1.0$. The dashed line is the leading order approximation, that is, function γ^2 is a constant $(\gamma^{(0)})^2$ for all frequencies. If we consider the solid line from paper [19] as an exact solution, then the errors between two lines increase as frequency increases. The relative error is up to 16% when $f = 16GHz$. The dotted line with stars is the quadratic approximation by using equation (4.34). This is a good approximation when f is small. From the plot, we observe that the relative error is less than 2% when f is less than $10GHz$. When $f = 10Ghz$, parameter δ is 0.2. Therefore, the quadratic approximation is a good approximation when δ is small comparing to 1. However, when f is big enough so

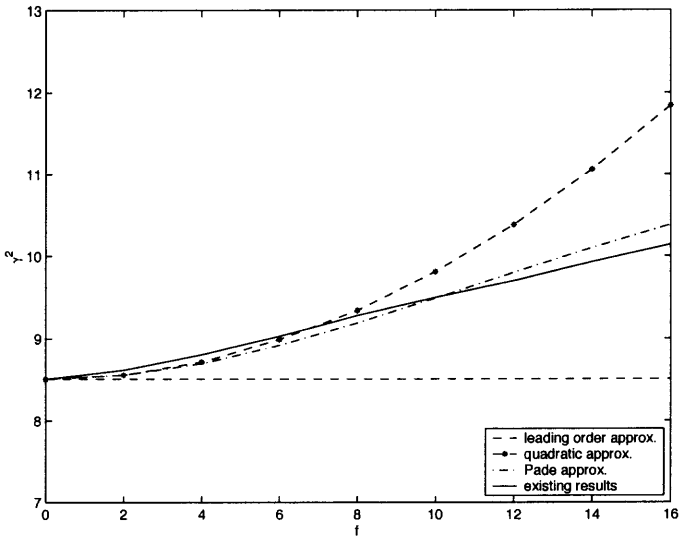

Figure 5.6 The plot of function γ^2 for different approximations, $N_1^2 = 12.9$, $a = 1$.

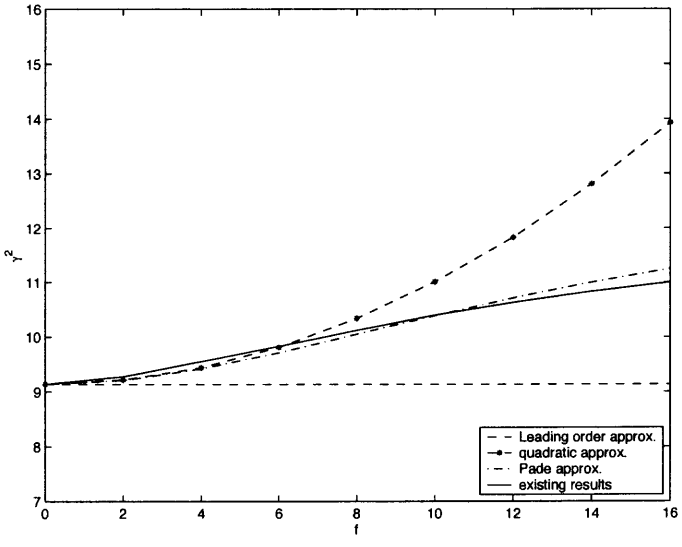

Figure 5.7 The plot of function γ^2 for different approximations, $N_1^2 = 12.9$, $a = 2$.

that δ cannot be considered as a small parameter, the quadratic approximation is not appropriate any more. The dash-dot line is the result by using Padé approximation. It corrects the behavior of the quadratic approximation at high frequencies and reduces the relative error to 3% at $f = 16GHz$. In Figure 5.7, same results are shown for $w/h = 2.0$.

In computing $\gamma^{(2)}$, we used half shielded Green's function because the half space Greens' function does not work. Therefore, we cannot compare the results obtained through these two Green's functions. However, we showed that this half shielded Green's function yields satisfying results by comparing our output with the existing ones. Therefore, it indirectly proves the validity of the half shielded Green's function in our approach.

CHAPTER 6

PERTURBATION ANALYSIS TO OTHER CONFIGURATIONS

In Chapter 4, we observe that by using perturbation analysis, it is natural to derive a quasi-TEM wave in a microstrip transmission line. Because of the existence of this quasi-TEM wave, microstrip can be described by capacitance, inductance and transmission line equations in microwave engineering. In this chapter, we will use the same analysis to derive transmission line equations for microstrip with smoothly changed width and coupled microstrip transmission lines. We will see that without using the equivalent circuit, the transmission line equations which describe the voltages and the currents of microstrip transmission lines are able to be deduced mathematically and each term of capacitances and inductances in the equations is well defined.

6.1 A Microstrip Transmission Line with a Smoothly Changing Width

We have applied perturbation analysis to a microstrip transmission line with a uniform strip width. This analysis can be generalized to the case when the width of the strip changes along the propagation direction. The results are very useful in the microstip matching networks.

When the width a is a function of z, the propagation constant γ is a function of z as well. Therefore, the z dependence of the solutions to the Maxwell equations is not simply $e^{-i\gamma z}$, as what we did in Chapter 4. When we take the derivative in equations (4.2) with respect to z, it cannot be simply written as a function multiplied

by $-i\gamma$. Therefore, equations (4.2) are written in their general forms as

$$E_{3y} - \delta E_{2z} = i\delta H_1, \tag{6.1a}$$

$$-E_{3x} + \delta E_{1z} = i\delta H_2, \tag{6.1b}$$

$$E_{2x} - E_{1y} = i\delta H_3, \tag{6.1c}$$

$$H_{3y} - \delta H_{2z} = -iN^2\delta E_1, \tag{6.1d}$$

$$-H_{3x} + \delta H_{1z} = -iN^2\delta E_2, \tag{6.1e}$$

$$H_{2x} - H_{1y} = iN^2\delta E_3. \tag{6.1f}$$

The regular asymptotic expansions of the electromagnetic fields E and H in (4.3a) and (4.3b) are substituted in these six equations. For each order of δ, we obtain a system of equations. The zeroth order equations yield $E_3^0 = H_3^0 \equiv 0$ by the same reasoning as we did for a uniform strip line.

The first order equations are stated as

$$E_{3y}^{(1)} - E_{2z}^{(0)} = iH_1^{(0)}, \tag{6.2a}$$

$$-E_{3x}^{(1)} + E_{1z}^{(0)} = iH_2^{(0)}, \tag{6.2b}$$

$$E_{2x}^{(0)} - E_{1y}^{(0)} = 0, \tag{6.2c}$$

$$H_{3y}^{(1)} - H_{2z}^{(0)} = -iN^2E_1^{(0)}, \tag{6.2d}$$

$$-H_{3x}^{(1)} + H_{1z}^{(0)} = -iN^2E_2^{(0)}, \tag{6.2e}$$

$$H_{2x}^{(0)} - H_{1y}^{(0)} = 0. \tag{6.2f}$$

Hence, functions $E_1^{(0)}$ and $E_2^{(0)}$ still satisfy equations (4.8). We set $E_1^{(0)} = -\Phi_0(z)\Phi_x$ and $E_2^{(0)} = -\Phi_0(z)\Phi_y$. In this representation Φ is defined the same way as before for fixed z, that is, Φ satisfies Laplace equation and takes the value 1 on the strip and 0 on the ground plane. However, since the strip width is a function of z, the solution of Φ also depends on z. The unknown function Φ_0 takes into account the changing of the potential on the strip along the z direction.

The equations for $H_1^{(0)}$ and $H_2^{(0)}$ are (4.10). Therefore, we set $H_1^{(0)} = \hat{\Psi}_y$ and $H_2^{(0)} = -\hat{\Psi}_x$ such that $\nabla^2\hat{\Psi} = 0$ and $\hat{\Psi}$ is a constant on both the strip and the ground plane for fixed z. Substituting the potential representations of $E_1^{(0)}$, $E_2^{(0)}$, $H_1^{(0)}$ and $H_2^{(0)}$ in equations (6.2a) and (6.2b), we obtain

$$E_3^{(1)} = i\hat{\Psi} - \Phi_{0z}\Phi - \Phi_0\Phi_z. \tag{6.3}$$

Since $E_3^{(1)}$ is 0 on both the strip and the ground plane and Φ equals 1 on the strip and 0 on the ground plane, equation (6.3) determines that function $\hat{\Psi}$ is $-i\Phi_{0z}$ on the strip and takes the value 0 on the ground plane. Therefore, we let $\hat{\Psi} = -i\Phi_{0z}\Psi$, where function Ψ is defined in the same way as in Chapter 4. This changing of variable gives $H_1^{(0)} = -i\Phi_{0z}\Psi_y$ and $H_2^{(0)} = i\Phi_{0z}\Psi_x$.

Substituting $H_1^{(0)} = -i\Phi_{0z}\Psi_y$ and $E_2^{(0)} = -\Phi_0(z)\Phi_y$ in equation (6.2e) and employing the same argument as we used to deduce $(\gamma^{(0)})^2$ yields a differential equation for $\Phi_0(z)$,

$$\frac{\partial}{\partial z}\{\frac{1}{l(z)}\Phi_{0z}\} + C(z)\Phi_0 = 0, \tag{6.4}$$

where

$$\begin{aligned} l(z) &= \frac{1}{\int_{s(z)}[\Psi_y]dx} \\ C(z) &= \int_{s(z)}[N^2\Phi_y]dx. \end{aligned} \tag{6.5}$$

In equation (6.5), $\int_{s(z)}$ denotes the integral over the strip (the width of the strip is a function of z). Integrands $[N^2\Phi_y]$ and $[\Psi_y]$ also depend on the width of the strip. When the strip has uniform width, the equation for Φ_0 becomes

$$\Phi_{0zz} + lC\Phi_0 = 0. \tag{6.6}$$

which gives the first order propagation constant defined in (4.14), that is, $\gamma^{(0)} = \sqrt{lC}$.

Equation (6.4) is a transmission line equation for the potentials on the strip with

arbitrary width. The integrals in (6.5) are known functions of the strip width (see Figure 5.3). Hence, if we prescribe the width as a function of z, the l and C are known and the equation (6.4) can be solved numerically. However, if we assume that the with of the strip changes slowly comparing with the wavelength, then the WKB method can be applied to find an approximation solution of Φ_0, that is,

$$\Phi_0 = A_0 \frac{\sqrt{l(\epsilon z)}}{\sqrt{\gamma^{(0)}(\epsilon z)}} e^{\frac{i}{\epsilon}\int^{\epsilon z}\gamma^{(0)}(z')dz'} + B_0 \frac{\sqrt{l(\epsilon z)}}{\sqrt{\gamma^{(0)}(\epsilon z)}} e^{\frac{-i}{\epsilon}\int^{\epsilon z}\gamma^{(0)}(z')dz'}. \tag{6.7}$$

In this solution, ϵ is a small parameter defined by D/λ_0, where D is the characteristic length on which the strip width changes in the z direction. Unknown coefficients A_0 and B_0 are chosen according to the boundary conditions at the source and the load. For a matching network, we need a maximum power delivered into the network and no reflection at the load [12]. If the source impedance and the load impedance are R_S and R_L, respectively, these two conditions yield $l(L/D)/C(L/D) = R_L$ at the load and $l(0)/C(0) = R_s^*$ at the source.

6.2 The Derivation of Coupled Microstrip Transmission Line Equations

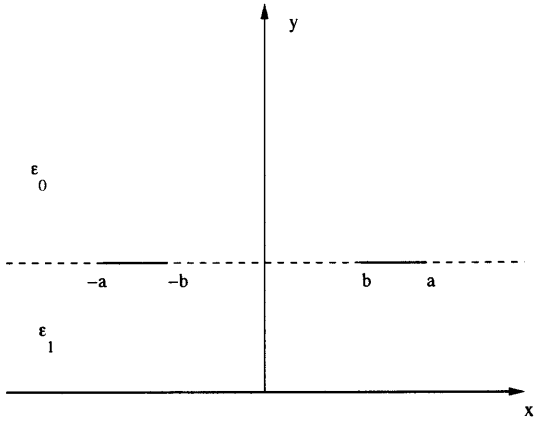

Figure 6.1 Coupled microstrip transmission lines.

The perturbation analysis that we have applied to a single microstrip, can be naturally extended to deal with coupled microstrip transmission lines.

Figure 6.1 is a diagram of coupled microstrip transmission lines. Two strips are uniform along the z direction. The same nondimensionalization is done as we did for single microstrip, and the six scalar Maxwell equations are (6.1) with different boundary conditions. When we do the same perturbation analysis, the zeroth order equations give: $E_3^{(0)} = H_3^{(0)} \equiv 0$, which means a quasi-TEM wave is supported by this structure.

The first order equations are (6.2). So the equations for $E_1^{(0)}$ and $E_2^{(0)}$ are follows,

$$(N^2 E_1^{(0)})_x + (N^2 E_2^{(0)})_y = 0 \tag{6.8a}$$

$$E_{2x}^{(0)} - E_{1y}^{(0)} = 0. \tag{6.8b}$$

We let $E_1^{(0)} = -\Phi_x$ and $E_2^{(0)} = -\Phi_y$, then this Φ satisfies

$$\nabla(N^2 \nabla \Phi) = 0, \tag{6.9}$$

and equals Φ_1 on the left strip and Φ_2 on the right strip. Both Φ_1 and Φ_2 are unknown potentials. Across the air-dielectric interface, both Φ and $N^2\Phi_y$ are continuous. In order to find the equations for Φ_1 and Φ_2, we write Φ as an linear combination of two functions, that is,

$$\Phi = \Phi_1 \varphi_{10} + \Phi_2 \varphi_{01}. \tag{6.10}$$

In this equation (6.10), both functions φ_{10} and φ_{01} satisfy (6.9) and continuous across the interface. Function φ_{10} takes the value 1 on the left strip and 0 on the right strip, while function φ_{01} takes the value 0 on the left strip and 1 on the right strip. Both of the functions are 0 on the ground plane. In brief, the subscripts of the φ_{01} and φ_{10} stand for the values of the potentials on each strip. These two functions are considered as basis functions to the problem. Their values can be found numerically. Potentials Φ_1 and Φ_2 are constants for fixed z on the strips and are functions of z

only. By this decomposition of Φ, the E components can be written as

$$E_1^{(0)} = -\Phi_1(z)(\varphi_{10})_x - \Phi_2(z)(\varphi_{01})_x, \tag{6.11a}$$

$$E_2^{(0)} = -\Phi_1(z)(\varphi_{10})_y - \Phi_2(z)(\varphi_{01})_y. \tag{6.11b}$$

Thus, if we determine Φ_1 and Φ_2, then the transverse electrical fields are given by these two equations.

Functions H_1^0 and H_2^0 satisfy equations

$$H_{1x}^{(0)} + H_{2y}^{(0)} = 0, \tag{6.12a}$$

$$H_{2x}^{(0)} - H_{1y}^{(0)} = 0. \tag{6.12b}$$

Let $H_1^{(0)} = \Psi_y$ and $H_1^{(0)} = -\Psi_x$. Then, from these two equations and the boundary conditions, Ψ satisfies Laplace equation and is continuous across the air-dielectric interface. The values of Ψ on two strips and the ground plane can be derived from $E_3^{(1)}$ which connects function Ψ to the unknown potentials Φ_1 and Φ_2. Substituting potential representations of the electromagnetic fields in equations (6.2a) and (6.2b) yields two equations for $E_3^{(1)}$, which are integrated to give

$$E_3^{(1)} = -\Phi_{1z}\varphi_{10} - \Phi_{2z}\varphi_{01} + i\Psi. \tag{6.13}$$

Since E_3 is 0 on metal surfaces, by applying the values of φ_{10} and φ_{01} on the strips and on the ground plane, the values of Ψ on these surfaces are then deduced as: $\Psi = -i\Phi_{1z}$ on the left strip, $\Psi = -i\Phi_{2z}$ on the right strip and $\Psi = 0$ on the ground plane. Doing the same decomposition to Ψ as we did for Φ, we take

$$\Psi = -i\Phi_{1z}\psi_{10} - i\Phi_{2z}\psi_{01} \tag{6.14}$$

in which ψ_{10} and ψ_{01} are two basis functions similar as φ_{10} and φ_{01}. They satisfy Laplace equations and are continuous across the air-dielectric interface. On the

ground plane, both of them are 0; on the strips, ψ_{10} takes the value 1 and 0, while ψ_{01} takes the value 0 and 1. Although functions ψ_{10} and ψ_{01} do not have analytical solutions, they can be accurately approximated by many numerical methods. In terms of potential functions, the transverse magnetic fields can be written as

$$H_1^{(0)} = -i\Phi_{1z}(z)(\psi_{10})_y - i\Phi_{2z}(z)(\psi_{01})_y, \tag{6.15a}$$

$$H_2^{(0)} = i\Phi_{1z}(z)(\psi_{10})_x + i\Phi_{2z}(z)(\psi_{01})_x. \tag{6.15b}$$

In the remainder of this section, we will deduce transmission line equations for the coupled microstrip transmission lines.

Since the leading order Maxwell equations (6.2) describe a quasi-TEM wave, we can define current for this case. If the current along the left strip is $I_1(z)$ and the current along the right strip is $I_2(z)$, then they are related to the H field in the following way:

$$I_1 = \int_{s_1} [H_1^{(0)}]dx, \tag{6.16a}$$

$$I_2 = \int_{s_2} [H_1^{(0)}]dx, \tag{6.16b}$$

where $\int_{s_1}$ and $\int_{s_2}$ denote the integration over the left and the right strips, respectively. Substituting (6.15a) in these two current equations and applying the continuity conditions of ψ_{10} and ψ_{01} across the air-dielectric interface, we obtain

$$I_1 = -i\Phi_{1z}\int_{s_1}[(\psi_{10})_y]dx - i\Phi_{2z}\int_{s_1}[(\psi_{01})_y]dx, \tag{6.17a}$$

$$I_2 = -i\Phi_{1z}\int_{s_2}[(\psi_{10})_y]dx - i\Phi_{2z}\int_{s_2}[(\psi_{01})_y]dx. \tag{6.17b}$$

We define: $l_{11} = 1/\int_{s_1}[(\psi_{10})_y]dx$, $l_{21} = 1/\int_{s_1}[(\psi_{01})_y]dx$, $l_{12} = 1/\int_{s_2}[(\psi_{10})_y]dx$ and $l_{22} = 1/\int_{s_2}[(\psi_{01})_y]dx$, then equations (6.17) for the currents are simplified as

$$I_1 = -\frac{i}{l_{11}}\Phi_{1z} - \frac{i}{l_{21}}\Phi_{2z}, \tag{6.18a}$$

$$I_2 = -\frac{i}{l_{12}}\Phi_{1z} - \frac{i}{l_{22}}\Phi_{2z}. \tag{6.18b}$$

The unknown functions Φ_{1z} and Φ_{2z} are then solved from these two equations,

$$\Phi_{1z} = \frac{il_{11}}{\nu_1}I_1 + \frac{il_{12}}{\nu_2}I_2 \tag{6.19a}$$

$$\Phi_{2z} = \frac{il_{21}}{\nu_2}I_1 + \frac{il_{22}}{\nu_1}I_2, \tag{6.19b}$$

where $\nu_1 = 1 - l_{11}l_{22}/l_{12}l_{21}$ and $\nu_2 = 1 - l_{21}l_{12}/l_{11}l_{22}$ are dimensionless quantitiess which are not zero. In addition, if the strips are symmetric, then $l_{11} = l_{22}$ and $l_{12} = l_{21}$, that is, the coefficient matrix in equations (6.19) is symmetric.

Equations (6.19) have four unknowns, Φ_1, Φ_2, I_1 and I_2. In order to find another two equations involving these four unknowns, we consider the leading order equation (6.2e), which is

$$H_{1z}^{(0)} = H_{3x}^{(1)} - iN^2E_2^{(0)}. \tag{6.20}$$

Integrating this equation from $-\infty$ to 0 at y=1^+ and y=1^- yields respectively,

$$\int_{-\infty}^{0} H_{1z}^{(0)}|_{y=1^+}dx = H_3^{(1)}(-\infty, 1^+) - H_3^{(0)}(0, 1^+) - i\int_{-\infty}^{0} N^2E_2^{(0)}|_{y=1^+}dx, \tag{6.21a}$$

$$\int_{-\infty}^{0} H_{1z}^{(0)}|_{y=1^-}dx = H_3^{(1)}(-\infty, 1^-) - H_3^{(0)}(0, 1^-) - i\int_{-\infty}^{0} N^2E_2^{(0)}|_{y=1^-}dx. \tag{6.21b}$$

Changing the order of z derivative and the integration on the left hand sides of these two equations and subtracting one from the other, we obtain

$$\frac{d}{dz}\int_{s_1}[H_1^{(0)}]dx = -i\int_{s_1}[N^2E_2^{(0)}]dx, \tag{6.22}$$

where we applyed the continuity conditions of functions $H_3^{(0)}$ and $N^2E_2^{(0)}$ across the air-dielectric interface. Substituting equations (6.16a), (6.11b) in equation (6.22) gives

$$I_{1z} = i\Phi_1 \int_{s_1} [N^2(\varphi_{10})_y]dx + i\Phi_2 \int_{s_1} [N^2(\varphi_{01})_y]dx. \tag{6.23}$$

We define $C_{11} = \int_{s_1}[N^2(\varphi_{10})_y]dx$ and $C_{21} = \int_{s_1}[N^2(\varphi_{01})_y]dx$. Therefore, equation for I_{1z} is simplified as

$$I_{1z} = iC_{11}\Phi_1 + iC_{21}\Phi_2. \tag{6.24}$$

Similarly, we integrate equation (6.20) from 0 to ∞ and repeat this procedure, we deduce

$$I_{2z} = iC_{12}\Phi_1 + iC_{22}\Phi_2, \tag{6.25}$$

where $C_{12} = \int_{s_2}[N^2(\varphi_{10})_y]dx$ and $C_{22} = \int_{s_2}[N^2(\varphi_{01})_y]dx$. If the coupled strips are symmetric about the y axis, then we have $C_{11} = C_{22}$ and $C_{12} = C_{21}$.

Equations (6.19a), (6.19b), (6.24), (6.25) are first order differential equations for the currents and the voltages on the two strips. They are the same equations as those derived by using equivalent circuits [2] [38].

The coefficients of the four coupled first order differential equations are functions of l and C's. These l and C's are dependent on the basis functions with which we chose to express the potential functions Φ and Ψ. Therefore, if we change the basis functions, for example, if we choose φ_{even} and φ_{odd} as the basis functions for Φ, (that is, for φ_{even} both the strips have constant 1 and for φ_{odd} left strip equals 1 and right strip equals -1), then we will have different combinations of different l and C's in the coefficient matrix. However, the two coefficient matrices that are obtained through different bases are identical since the solutions of the voltages and the currents on the strips are unique.

6.3 Conclusion

In Chapters 4, 5 and 6, we discussed the problem of a microstip transmission line by applying a perturbation analysis. We assumed that the thickness of the strip is negligible, and the substrate is an isotropic dielectric. We considered the case when the wavelength is much larger than the height of the substrate, and the width of the strip is the same order as the height of the substrate. Under these assumptions, we nondimensionalized Maxwell's equations and introduced a small parameter $\delta = 2\pi h/\lambda_0$. Then the components of the electromagnetic fields and the propagation constant γ were expanded in a regular asymptotic expansion. Groups of differential equations with the same order of δ were solved mathematically by introducing proper potential functions. These potential functions are elliptic in character and are coupled through boundary conditions of the longitudinal electrical field. The solvability conditions for the longitudinal magnetic field yield the propagation constant of each order. The perturbation analysis was carried out until the third order propagation constant was found. It turned out that the propagation constant is an even function of f at low frequencies. For arbitrary f, the behavior of the propagation constant was derived by using the Padé approximation and the information from both the low frequency expansion and the high frequency limit.

Through the derivation, we mathematically verified that at low frequencies, microstrip transmission line supports a quasi-TEM wave. That is, the longitudinal electromagnetic fields are very small comparing to the transverse electromagnetic fields. However, the longitudinal fields are very important and cannot be neglected in deriving boundary conditions of potential problems and in deriving the expression of the propagation constant.

All derived potentials have been solved numerically by converting the Laplace equations into integral equations through appropriate Green's function representations. Both the half space Green's function and the half shielded Green's function were used

to give the results of the leading order propagation constant. The differences are not distinct. Therefore, in finding $\gamma^{(2)}$ we used a half shielded Green's function instead of a half space Green's function to overcome the numerical difficulty in dealing with an unbounded domain. The results showed satisfactory agreement with other existing solutions.

The same perturbation analysis was generalized to deal with a single strip with changing widths and with coupled microstrip transmission lines. In both cases, transmission line equations were derived and each coefficient in the equations were well defined through potential functions. For the single microstrip transmission line with slowly changed widths, the potential on the strip was solved by the WKB method and results are applicable to microwave matching network. For coupled microstrip transmission lines, the transmission line equations were derived without using the equivalent circuits. The same analysis can be modified to deal with transmission lines with more than two strips and with other configurations.

APPENDIX A

THE ORDER OF EIGENVALUES AND EIGENFUNCTIONS

In this appendix we will find the order of eigenvalues and eigenfunctions of a general hole shape. The characteristic size of the hole is d which is defined as the square root of the area of the hole. We assume that the eigenvalues and the eigenfunctions are λ_p and φ_p respectively, with $p = 0, 1, 2 \cdots$. It is known that for each p

$$\iint_H \varphi_p^2(x,y)dxdy = 1 \tag{A.1}$$

by the othonormality of the eigenfunctions. The average value of function φ_p^2 over the area S is defined by $\frac{1}{d^2}\iint_s \varphi_p^2(x,y)dxdy$, which is $1/d^2$. Therefore, the average value of function φ_p over the hole is $1/d$. If we let

$$\varphi_p(x,y) = \frac{1}{d}\tilde{\varphi}_p(x,y), \tag{A.2}$$

then the average value of function $\tilde{\varphi}_p$ over the hole is 1.

Eigenfunctions φ_p satisfy equation

$$\nabla^2\varphi_p(x,y) = -\lambda_p^2\varphi_p(x,y). \tag{A.3}$$

Multiplying this equation by φ_p on both sides and applying the divergence theorem and the boundary conditions yields

$$\lambda_p^2 = \frac{\iint_H |\nabla\varphi_p|^2 dxdy}{\iint_H \varphi_p^2(x,y)dxdy} = \iint_H |\nabla\varphi_p|^2 dxdy = O(1/d^2) \tag{A.4}$$

since eigenfunctions φ_p are $O(1/d)$ functions. Then, we rewrite λ_p as $\lambda_p = \frac{1}{d}\tilde{\lambda}_p$ with $\tilde{\lambda}_p$ being order one.

APPENDIX B

THE PROOF OF THE RECIPROCAL PROPERTY

To prove $\gamma_{00} = \tau_0$, let's consider equation

$$\nabla \cdot \{u_2 \nabla u_1 - u_1 \nabla u_2\} = 0. \tag{B.1}$$

Integrating it over the cube $|z| < z_\infty$, $|x| < a/2$, $|y| < b/2$ and applying the divergence theorem, we obtain

$$\iint (u_2 \frac{\partial u_1}{\partial n} - u_1 \frac{\partial u_2}{\partial n}) ds = 0, \tag{B.2}$$

where the double integral is over the six surfaces of the cube and n is the normal direction of each surface. The integrals over four surfaces cancel off with each other because of the periodic boundary conditions. Therefore, only the surface integrals over the top and the bottom remain, which gives

$$\int_{-a/2}^{a/2} \int_{-b/2}^{b/2} (u_2 \frac{\partial u_1}{\partial z} - u_1 \frac{\partial u_2}{\partial z})|_{z=-\infty} dx dy = \iint_H (u_2 \frac{\partial u_1}{\partial z} - u_1 \frac{\partial u_2}{\partial z})|_{z=\infty} ds. \tag{B.3}$$

After substituting infinite series expansions for u_1 and u_2 in this equation, most terms cancel off. We obtain

$$2ik\gamma_{00} = 2ik\tau_0, \tag{B.4}$$

which yields the result $\gamma_{00} = \tau_0$.

APPENDIX C

THE PROPERTY OF THE SCATTERING MATRIX

Suppose we chose k properly such that all the higher order modes are evanescent. Then, generally, we have $u_1 = a_0 e^{-ikz} + b_0 e^{ikz}$ at $z = -\infty$ and $u_1 = c_0 e^{ikz} + d_0 e^{-ikz}$ at $z = \infty$. Considering $\nabla \cdot \{\bar{u_1} \nabla u_1 - u_1 \nabla \bar{u_1}\} = 0$, which is equivalent to $\nabla \cdot \{\Im(\bar{u_1} \nabla u_1)\} = 0$, by using the same procedure as was done in Appendix A, we obtain

$$\int_{-a/2}^{a/2} \int_{-b/2}^{b/2} \Im(\bar{u_1} \frac{\partial u_1}{\partial z})|_{z=-\infty} dxdy = \iint_H \Im(\bar{u_1} \frac{\partial u_1}{\partial z})|_{z=\infty} ds. \tag{C.1}$$

Substituting the expression of u_1 at $z = \pm\infty$ in equation (C.1) yields

$$|a_0|^2 + |c_0|^2 = |b_0|^2 + |d_0|^2. \tag{C.2}$$

We know that a_0, b_0, c_0 and d_0 are related by matrix S_1, that is

$$b_0 = (1 - d\tau_0)a_0 + \tau_0 c_0 \tag{C.3a}$$

$$d_0 = \tau_0 a_0 + (1 - \tau_0/d)c_0. \tag{C.3b}$$

Inserting them into equation (C.2) gives

$$\begin{aligned} &\{|1 - d\tau_0|^2 + |\tau_0|^2 - 1\}|a_0|^2 + \{|1 - \tau_0/d|^2 + |\tau_0|^2 - 1\}|c_0|^2 \\ &+ 2\Re\{(1 - d\bar{\tau}_0)\tau_0 \bar{a}_0 c_0 + (1 - \tau_0/d)\bar{\tau}_0 \bar{a}_0 c_0\} = 0. \end{aligned} \tag{C.4}$$

Setting $a_0 = 1$, $c_0 = 0$ and $a_0 = 0$, $c_0 = 1$, respectively, we have three equations

$$|1 - d\tau_0|^2 + |\tau_0|^2 = 1, \tag{C.5a}$$

$$|1 - \tau_0/d|^2 + |\tau_0|^2 = 1, \tag{C.5b}$$

$$\tau_0 + \bar{\tau}_0 - d|\tau_0|^2 - |\tau_0|^2/d = 0, \tag{C.5c}$$

which prove that $S_1 \cdot S_1^T = I$.

APPENDIX D

THE COMPUTATION OF Z_{MN}

To calculate Z_{mn}, we first rewrite the Green's function as

$$G(x,y,0|x',y',0) = \frac{1}{ik} + \sum_{n=1}^{\infty} \frac{2}{i\beta_{0n}} \cos 2n\pi(y-y')/b + \sum_{m=1}^{\infty} \frac{2}{i\beta_{m0}} \cos 2m\pi(x-x')/a + \sum_{m=1}^{\infty}\sum_{n=1}^{\infty} \frac{4}{i\beta_{mn}} \cos 2m\pi(x-x')/a \cos 2n\pi(y-y')/b. \tag{D.1}$$

Then we interchange the summation and integral in the definitions of Z_{mn}. The integrals are evaluated by using the formulae listed as follows [1]:

$$\int_0^{\pi} \cos(x\sin\theta)d\theta = \int_0^{\pi} \cos(x\cos\theta)d\theta = \pi J_0(x), \tag{D.2a}$$

$$\int_0^{a} xJ_0(x)dx = aJ_1(a), \tag{D.2b}$$

$$\int tJ_\mu(kt)J_\gamma(lt)dt = \frac{t}{k^2-l^2}\{kJ_{\mu+1}(kt)J_\gamma(lt) - lJ_\mu(kt)J_{\gamma+1}(lt)\}. \tag{D.2c}$$

APPENDIX E

THE RANGE OF $\gamma^{(0)}$

This appendix gives the proof that $1 < (\gamma^{(0)})^2 < N_1^2$. Let's first consider the identity

$$\nabla \cdot (\Psi \nabla \Psi) = \nabla \Psi \cdot \nabla \Psi, \tag{E.1}$$

which is true since $\nabla^2 \Psi = 0$. Integrating (E.1) over Region I and Region II, respectively and applying the corresponding boundary conditions yields:

$$-\int_{-\infty}^{\infty} \Psi \Psi_y|_{y=1^+} dx = \int_{-\infty}^{\infty} \int_{1}^{\infty} |\nabla \Psi|^2 dxdy \tag{E.2a}$$

$$\int_{-\infty}^{\infty} \Psi \Psi_y|_{y=1^-} dx = \int_{-\infty}^{\infty} \int_{0}^{1} |\nabla \Psi|^2 dxdy. \tag{E.2b}$$

Adding these two equations gives

$$-\int_s [\Psi_y] dx = \int_{-\infty}^{\infty} \int_{0}^{\infty} |\nabla \Psi|^2 dxdy, \tag{E.3}$$

since Ψ and Ψ_y are continuous across the interface and $\Psi = 1$ on the strip. The same procedure are applied to three other indentities

$$\nabla \cdot (\Phi \nabla \Psi) = \nabla \Phi \cdot \nabla \Psi, \tag{E.4a}$$

$$\nabla \cdot (\Psi N^2 \nabla \Phi) = N^2 \nabla \Phi \cdot \nabla \Psi, \tag{E.4b}$$

$$\nabla \cdot (\Phi N^2 \nabla \Phi) = N^2 \nabla \Phi \cdot \nabla \Phi, \tag{E.4c}$$

to deduce

$$-\int_s [\Psi_y] dx = \int_{-\infty}^{\infty} \int_{0}^{\infty} \nabla \Phi \cdot \nabla \Psi dxdy, \tag{E.5a}$$

$$-\int_s [N^2 \Phi_y] dx = \int_{-\infty}^{\infty} \int_{0}^{\infty} N^2 \nabla \Phi \cdot \nabla \Psi dxdy, \tag{E.5b}$$

$$-\int_s [N^2 \Phi_y] dx = \int_{-\infty}^{\infty} \int_{0}^{\infty} N^2 |\nabla \Phi|^2 dxdy. \tag{E.5c}$$

Therefore, by applying these four equations (E.3) and (E.5) and the Cauchy-Schwarz inequality, we have the following derivation:

$$\begin{aligned}
\left(\int_s [N^2\Phi_y]dx\right)^2 &= \left(\int_{-\infty}^{\infty}\int_0^{\infty} N\nabla\Phi\cdot N\nabla\Psi dxdy\right)^2 \\
&\le \int_{-\infty}^{\infty}\int_0^{\infty} N^2|\nabla\Phi|^2 dxdy \int_{-\infty}^{\infty}\int_0^{\infty} N^2|\nabla\Psi|^2 dxdy \\
&= \left(-\int_s [N^2\Phi_y]dx\right)\int_{-\infty}^{\infty}\int_0^{\infty} N^2|\nabla\Psi|^2 dxdy \\
&\le \left(-\int_s [N^2\Phi_y]dx\right) N_1^2 \int_{-\infty}^{\infty}\int_0^{\infty} |\nabla\Psi|^2 dxdy \\
&= N_1^2\left(\int_s [N^2\Phi_y]dx\right)\left(\int_s [\Psi_y]dx\right),
\end{aligned}$$

which gives $(\gamma^{(0)})^2 \le N_1^2$. Similarly, $1 \le (\gamma^{(0)})^2$ can be proved by the following arguments:

$$\begin{aligned}
\left(\int_s [\Psi_y]dx\right)^2 &= \left(\int_{-\infty}^{\infty}\int_0^{\infty} \nabla\Phi\cdot\nabla\Psi dxdy\right)^2 \\
&\le \int_{-\infty}^{\infty}\int_0^{\infty} |\nabla\Phi|^2 dxdy \int_{-\infty}^{\infty}\int_0^{\infty} |\nabla\Psi|^2 dxdy \\
&\le \int_{-\infty}^{\infty}\int_0^{\infty} N^2|\nabla\Phi|^2 dxdy \int_{-\infty}^{\infty}\int_0^{\infty} |\nabla\Psi|^2 dxdy \\
&= \left(\int_s [N^2\Phi_y]dx\right)\left(\int_s [\Psi_y]dx\right).
\end{aligned}$$

APPENDIX F

A DERIVATION OF THE HALF-SPACE GREEN'S FUNCTION WITH DIELECTRIC

This appendix shows how to derive Green's function $G(x, 1|x', 1)$ defined in equation (5.1). Let's take the Fourier integral transform of G:

$$\tilde{G}(l) = \int_{-\infty}^{\infty} G(x, y) e^{ilx} dx,$$

then the PDE is transformed into an ODE

$$\frac{\partial}{\partial y}(N^2 \frac{\partial \tilde{G}}{\partial y}) - N^2 l^2 \tilde{G} = e^{ilx'} \delta(y - y').$$

If (x', y') is in Region I, the solution to this ODE is

$$\tilde{G} = \begin{cases} A \sinh(ly), & \text{if } 0 < y < y'; \\ B \sinh(ly - ly') + C \cosh(ly - ly'), & \text{if } y' < y < 1; \\ De^{-|l|(y-1)}, & \text{if } y > 1; \end{cases}$$

by using the fact that $G = 0$ on $y = 0$ and G approaches zero at ∞.

At $y = y'$, $[\tilde{G}] = 0$ and $[\tilde{G}_y] = \frac{e^{ilx'}}{N_1^2}$; at $y = 1$, $[\tilde{G}] = 0$ and $[N^2 \tilde{G}_y] = 0$. By satisfying these four continuity conditions we can determine A, B, C, D through four linear equations:

$$\begin{aligned} C &= A \sinh(ly'), \\ Bl &= Al \cosh(ly') + \frac{1}{N_1^2} e^{ilx'}, \\ D &= B \sinh(l - ly') + C \cosh(l - ly'), \\ -|l|D &= N_1^2 Bl \cosh(l - ly') + N_1^2 Cl \sinh(l - ly'). \end{aligned}$$

Therefore,

$$D = \frac{-e^{ilx'}\sinh(ly')}{|l|\sinh(l) + N_1^2 l\cosh(l)}.$$

So $G(x,1|x',y')$ can be found by taking the Fourier inverse transform:

$$\begin{aligned} G(x,1|x'y') &= \frac{1}{2\pi}\int_{-\infty}^{\infty} De^{-ilx}dx \\ &= \frac{-1}{2\pi N_1^2}\int_{-\infty}^{\infty} \frac{e^{il(x-x')}\sinh(ly')}{l(\cosh(l) + \frac{1}{N_1^2}\frac{|l|}{l}\sinh(l))}dl \\ &= \frac{-1}{\pi N_1^2}\int_0^{\infty} \frac{\cos(lx-lx')\sinh(ly')}{l(\cosh(l) + \frac{1}{N_1^2}\sinh(l))}dl. \end{aligned} \tag{F.1}$$

The denominator of the integrand in (F.1) can be rewritten as

$$\begin{aligned} \cosh(l) + \frac{1}{N_1^2}\sinh(l) &= \frac{1}{2}(e^l + e^{-l}) + \frac{1}{N_1^2}\frac{1}{2}(e^l - e^{-l}) \\ &= \frac{1}{2}e^l(1 + \frac{1}{N_1^2})(1 + \rho e^{-2l}), \end{aligned}$$

where $\rho = \frac{N_1^2-1}{N_1^2+1} < 1$. Substituting this equation in equation (F.1) gives:

$$\begin{aligned} G(x,1|x'y') &= \frac{-2}{\pi(N_1^2+1)}\int_0^{\infty} \frac{\cos(lx-lx')\sinh(ly')}{le^l(1+\rho e^{-2l})dl} \\ &= \frac{-2}{\pi(N_1^2+1)}\int_0^{\infty} \frac{\cos(lx-lx')\sinh(ly')}{l}e^{-l}\sum_{n=0}^{\infty}(-\rho)^n e^{-2nl}dl \\ &= \frac{-2}{\pi(N_1^2+1)}\sum_{n=0}^{\infty}(-\rho)^n\int_0^{\infty} \frac{\cos(ld)\sinh(ly')e^{-(2n+1)l}}{l}dl \\ &= \frac{-2}{\pi(N_1^2+1)}\sum_{n=0}^{\infty}(-\rho)^n I. \end{aligned} \tag{F.2}$$

In equation (F.2), we set $d = x - x'$ and interchanged the order of the summation and the integral.

To evaluate I, we let $a = (2n+1) \geqslant 1$, then I satisfies the following wave

equation and initial conditions:

$$\begin{aligned} I_{aa} &= I_{y'y'}, \\ I(a,0) &= 0, \\ I_{y'}(a,0) &= \int_0^\infty \cos(ld)e^{-al}dl = \frac{a}{a^2+d^2}. \end{aligned} \tag{F.3}$$

The solution to this wave equation is:

$$I = \frac{1}{4}\ln\left(\frac{(a+y')^2+d^2}{(a-y')^2+d^2}\right).$$

Hence, we can write $G(x,1|x',y')$ explicitly as

$$G(x,1|x',y') = \frac{1}{2\pi(N_1^2+1)}\sum_{n=0}^{\infty}(-\rho)^n \ln\left(\frac{(2n+1-y')^2+(x-x')^2}{(2n+1+y')^2+(x-x')^2}\right).$$

When the point (x',y') is in Region I, we will get the same expression for $G(x,1|x',y')$.

REFERENCES

[1] ABRAMOWITZ, M., AND STEGUN, I. A. *Handbook of mathematical functions with formulas, graphs, and mathematical tables.* Dover Publications, Inc. New York, 1972.

[2] ADAIR, J. E., AND HADDAD, G. I. Coupled-mode analysis of nonuniform coupled transmission lines. *IEEE Transactions on Microwave Theory and Techniques MTT-17*, 10 (1969), 746-752.

[3] AMARI, S., VAHLDIECK, R., AND BORNEMANN, J. Using selecting asymptotics to accelerate dispersion analysis of microstrip lines. *IEEE Transactions on Microwave Theory and Techniques 46*, 7 (1998), 1024-1027.

[4] ANDERSON, I. Comment on " remarkable transmission of microwaves through a wall of long metallic bricks". *Applied Physics Letters 82* (2003), 308-309.

[5] BARRETT, R. M. Microwave printed circuits-a history survey. *IEEE Transactions on Microwave Theory and Techniques MTT-3* (1955), 1-9.

[6] BRYANT, T. G., AND A., W. J. Parameters of microstrip transmission lines and of coupled pairs of microstrip lines. *IEEE Transactions on Microwave Theory and Techniques MTT-16*, 12 (1968), 1021-1027.

[7] COLLIN, R. E. *Field theory of Guided waves*, second ed. The Institute of Electrical and Electronics Engineerings, Inc., New York, 1990.

[8] DENLINGER, E. J. A frequency dependent solution for microstrip transmission lines. *IEEE Transactions on Microwave Theory and Techniques MTT-19*, 1 (1971), 30-39.

[9] EBBESEN, T. W., LEZEK, H. J., GHAEMI, H. F., THIO, T., AND WOLFF, P. A. Extraordinary optical transmission through sub-wavelength hole arrays. *Nature 391* (1998), 667-669.

[10] GETSINGER, W. J. Microstrip dispersion model. *IEEE Transactions on Microwave Theory and Techniques MTT-21*, 1 (1973), 34-39.

[11] GLADWELL, G. M., AND COEN, S. A chebyshev approximation method for microstrip problems. *IEEE Transactions on Microwave Theory and Techniques MTT-23*, 11 (1975), 865-870.

[12] GONZALEZ, G. *Microwave Transistor Amplifiers: Analysis and Design*, second ed. Prentice-Hall, Inc., New Jersey, 1997.

[13] HASHIMOTO, M. A rigorous soltion for disersive microstrip. *IEEE Transactions on Microwave Theory and Techniques MTT-31*, 11 (1985), 1131-1137.

[14] HIBBINS, A. P., AND SAMBLES, J. R. Remarkable transmission of microwaves through a long wall of metallic bricks. *Applied Physics Letters 79* (2001), 2844-2846.

[15] HIGGINS, T. J., AND BLACK, K. G. Rigorous determination of the parameters of microstrip transmission lines. *IEEE Transactions on Microwave Theory and Techniques MTT-3* (1955), 93-113.

[16] HORNSBY, J. S., AND GOPINATH, A. Numerical analysis of a dielectric-loaded waveguide with a microstrip line–finite-difference method. *IEEE Transactions on Microwave Theory and Techniques MTT-17*, 9 (1969), 684-690.

[17] JANSEN, R. H. High-speed computation of single and coupled microstrip parameters including dispersion, high-order modes, loss and finite strip thickness. *IEEE Transactions on Microwave Theory and Techniques MTT-26*, 2 (1978), 75-82.

[18] KOBAYASHI, M., AND ANDO, F. Dispersion characteristics of open microstrip lines. *IEEE Transactions on Microwave Theory and Techniques MTT-35*, 2 (1987), 101-105.

[19] KRETCH, B. E., AND COLLIN, R. E. Microstrip dispersion including anisotropic substrates. *IEEE Transactions on Microwave Theory and Techniques MTT-35*, 8 (1987), 710-718.

[20] KRIEGSMANN, G. A. Complete transmission through a two-dimensional diffraction grating. *accepted.*

[21] KUESTER, E. F., AND CHANG, D. C. Theory of dispersion in microstrip of arbitrary width. *IEEE Transactions on Microwave Theory and Techniques MTT-28*, 3 (1980), 259-265.

[22] MITTRA, R., AND ITOH, T. Spectral-domain approach for calculating the dispersion characteristics of microstrip lines. *IEEE Transactions on Microwave Theory and Techniques MTT-21* (1973), 496-499.

[23] MITTRA, R., AND ITOH, T. A technique for computing dispersion characteristics of shielded microstrip lines. *IEEE Transactions on Microwave Theory and Techniques MTT-22* (1974), 896-898.

[24] MITTRA, R., AND LEE, S. W. *Analytical techniques in the theory of guided waves.* The Macmillan Company, New York, 1971.

[25] NORRIS, A. N., AND LUO, H. A. Acoustic radiation and reflection from a periodically perforated rigid solid. *Journal of the Acoustical Society of America 82* (1987), 2113-2122.

[26] PANTIC, Z., AND MITTRA, R. Quasi-tem analysis of microstrip transmission lines by the finite element method. *IEEE Transactions on Microwave Theory and Techniques MTT-34* (1986), 1086-1103.

[27] PARK, S. O., AND BALANIS, C. Dispersion characteristics of open microstrip lines using closed-form asymptotic extraction. *IEEE Transactions on Microwave Theory and Techniques 45*, 3 (1997), 458-460.

[28] PORTO, J. A., GARCIA-VIDAL, F. J., AND PENDRY, J. B. Transmission resonances on metallic gratings with very narrow slits. *Physical Review Letters 83* (1999), 2845-2848.

[29] SCHNEIDER, M. B. Microstrip dispersion. *Proceedings of the IEEE* (Jan 1972), 144-146.

[30] SCHROTER, U., AND HEITMANN, D. Surface-plasmon-enhanced transmission through metallic gratings. *Physical Review B 58* (1998), 15419-15421.

[31] SHENG, P., STEPLEMAN, R. S., AND SANDA, P. N. Exact eigenfunctions for square-wave gratings: Application to diffraction and surface-plasmon calculations. *Physical Review B 26* (1982), 2907-2916.

[32] SHIH, C., WU, R., JENG, S., AND CHEN, C. A full-wave analysis of microstrip lines by variational conformal mapping technique. *IEEE Transactions on Microwave Theory and Techniques 36*, 3 (1988), 576-581.

[33] STINEHELFER, H. E. An accurate calculation of uniform microstrip transmission lines. *IEEE Transactions on Microwave Theory and Techniques MTT-16*, 7 (1968), 439-444.

[34] TSALAMENGAS, J. L., AND FIKIORIS, G. Rapidly converging spectral-domain analysis of rectangularly shielded layered microstrip lines. *IEEE Transactions on Microwave Theory and Techniques 51*, 6 (2003), 1729-1734.

[35] UCHIDA, K., NODA, T., AND MATSUNAGA, T. New type of spectral-domain analysis of a microstrip line. *IEEE Transactions on Microwave Theory and Techniques 37*, 6 (1989), 947-952.

[36] YAMASHITA, E. Variational method for the analysis of microstrip-like transmission lines. *IEEE Transactions on Microwave Theory and Techniques MTT-16*, 8 (1968), 529-535.

[37] YAMASHITA, E., AND MITTRA, R. Variational method for the analysis of microstrip lines. *IEEE Transactions on Microwave Theory and Techniques MTT-16*, 4 (1968), 251-256.

[38] YANG, Y. E., KONG, J. A., AND GU, Q. Time-domain perturbation analysis of nonuniformly coupled transmission lines. *IEEE Transactions on Microwave Theory and Techniques MTT-33*, 11 (1985), 1120-1130.